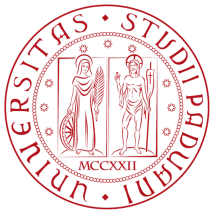

UNIVERSITÀ DEGLI STUDI DI PADOVA

Dipartimento di Ingegneria dell' Informazione

Corso di Laurea Magistrale in Control Systems Engineering

Tesi di Laurea

Rigidity theory in presence of noise for localization and control of multiagent systems

Relatore

prof. A. Cenedese

Correlatore

prof. G. Michieletto

Laureando

Marco Geremia

1241698

Anno Accademico 2021/2022

30 novembre 2022

Abstract

This thesis work aims at analyzing the formation, structure and response to noise the so-called bearing rigidity matrix, a mathematical tool applied in the fields of distributed control and estimation of multi-agent systems (e.g. UAV swarms or UGV fleets). At first, a basic theoretical background is established in order to better contextualize the experiments. Secondly, the aforementioned matrix is built using a soft-coded algorithmic approach and numerically simulated. Configuration-agnostic performance indices and descriptors are then established from an algebraic point of view in order to characterize the validity of the theoretical assumptions and the effect of the noise on the bearing measurements. Such measurements are simulated in a sequence of diverse fleet scenarios. The actual application of the bearing rigidity matrix in non-static scenarios concerning the efforts of control and estimation escapes the scope of this research and therefore will not be discussed in the following.

Sommario

Questo lavoro di tesi ha come obbiettivo quello di analizzare la costruzione, struttura e risposta al rumore della cosiddetta matrice di rigidità di bearing, uno strumento matematico utilizzato nei campi del controllo e della stima distribuiti di sistemi multi agenti (consistenti ad esempio in flotte di quadri rotori o robot terrestri a controllo remoto). Per prima cosa verrà stabilita una base teorica per meglio contestualizzare gli esperimenti eseguiti. Secondariamente la matrice di cui sopra verrà costruita in maniera programmatica secondo un approccio algoritmico soft-code e simulata numericamente. Una volta stabiliti indici di performance di carattere algebrico agnostici alla configurazione considerata, questi verranno utilizzati per stabilire la validità dei fondamenti teorici e valutare l'effetto del rumore nelle misurazioni. Tali misurazioni verranno simulate in una vasta sequenza di configurazioni di flotta. L'applicazione della matrice di rigidità di bearing in contesti dinamici riguardanti il controllo e la stima non rientra negli obbiettivi di questo testo e non verranno pertanto considerati in quanto segue.

Contents

List of Figures

List of Tables

Chapter 1

Introduction

1.1 Rigidity theory

Rigidity theory is a consolidated mathematical branch which investigates the structural rigidity (intuitively, the ability of resisting to an imparted disturbance) of grouping elements connected by some sort of linkage. In doing so, it crosses the fields of discrete geometry, rigid body mechanics and graph theory. Recently, this area of knowledge has found fertile ground in the field of distributed multi-agent control, assuming a whole new meaning encompassing the characterization of swarms of agents no longer physically coupled to one another but linked by means of sensing and communication capabilities.
In this newfound application, the various agents are assumed to be able to collect (in their local frame or by means of a centralized authority) some information regarding the spatial description of one another. This can be any kind of data, ranging from the most obvious distance to the more nuanced angles or bearing (which are normal constraints over the spatial direction linking the origin of each agent frame).
In any case, in order to describe a system of agents through rigidity theory, it is necessary to define a certain amount of elements which concur to establish the firm theoretical backbone of this discipline and are essential in understanding the meaning of the bearing rigidity matrix, which is the essence of this work.

The notion of framework

Once ascertained having a group of elements, each one of them must have a spatial characterization in terms of position. Each agent is assumed either as a particle or as a rigid body represented by its center of mass (CoM), described by an element of $\mathbb{R}^d, d \in \{1..3\}$. Additionally, one can also describe the agent orientation in the space by means of a coordinate frame with origin in the CoM. The choice of the space appropriate for such a description depends entirely on the characteristics of the agents itself.
As an example, in describing a UGV which can only move in a planar fashion and has a pose which can be described by means of a single angle $\theta \in [0, 2\pi)$ (its heading direction), one can use $\mathbb{R}^2$ for its position and the so-called special orthogonal group $SO(2) = \{\mathbf{R} \in \mathbb{R}^{2\times 2} \,|\mathbf{R}\mathbf{R}^\mathbf{T} = \mathbf{I_2}, det(\mathbf{R}) = 1\}$ of appropriate rotation matrices, which is isomorphic to the one dimensional manifold $\mathbb{S}^1$ (unit sphere). The agent will therefore belong to the special Euclidean group $SE(2) = \mathbb{R}^2 \times SO(2)$.

Alternatively, a UAV with complete actuation can move along 3 directions and can vary its pose arbitrarily in space. Such an agent would be described as a point in the special Euclidean group $SE(3) = \mathbf{R}^3 \times SO(3)$, where the special orthonormal group $SO(3) = \{\mathbf{R} \in \mathbb{R}^{3\times3} \,|\mathbf{R}\mathbf{R}^{\mathbf{T}} = \mathbf{I_3}, det(\mathbf{R}) = 1\}$ defines a manifold which is not isomorphic to the 2-sphere, since $\mathbb{S}^2 = SO(3)/SO(2)$.

In order to describe the informational relations among the elements in the group, it is necessary to establish a *graph* in which each node is represented by an agent and each edge is represented by the relative information exchanged (in this case, the measurement). The edges can be directed or undirected depending on the nature of such measurement: a measure referring to each agent local frame is not symmetric (digraph), one referred to the global frame is symmetric (graph).

The definition of *framework* stems from the crossing of the two previous concepts.

Definition 1 (Configuration) *Consider a formation comprised of n agents. Assume each agent* $i \in \{1...n\}$ *is associated to a point in the differential manifold* $\mathcal{D}_i \subseteq SE(3)$.
Through the definition of a common global frame among the agents, the configuration $\mathcal{X}_i \in \mathcal{D}_i$ *of the i-th agent describes either the position of the agent (when modeled as a particle) or the pose (position + attitude) of the agent (when modeled as a rigid body).*

Definition 2 (Framework in $\hat{\mathcal{D}}$) *A framework embedded in a product differential manifold* $\hat{\mathcal{D}} = \prod_{i=1}^{n}, \mathcal{D}_i \subseteq SE(3)^n$ *consists on an ordered pair* $(\mathcal{G}, \mathcal{X})$*, which is a graph* $\mathcal{G} = (\mathcal{V}, \mathcal{E})$ *together with a configuration* $\mathcal{X} = (\mathcal{X}_1 \dots \mathcal{X}_n) \in \hat{\mathcal{D}}$ *which is a map* $\mathcal{X} : \mathcal{V} \to \hat{\mathcal{D}}$ *associating to the vertex set a formation configuration, namely* $v_i \to \mathcal{X}(v_i) := \mathcal{X}_i \in \mathcal{D}_i$.

In the following, all agents formations are considered *noncollinear*, meaning that all the agents are in different positions and do no lie along the same line in the global frame reference. It is worth noting that a formation can be either *homogenous* or *heterogeneous* whether all the agents belong to the same differential manifold.

Building the bearing function

Bearing rigidity only considers as measurements the relative bearing of agents, which represents the direction linking two agents normalized by the distance in between. This choice is mostly driven by the fact that this measurement can be carried out with relative ease using cameras and computer vision techniques. The measure is referred to the local frame and this means that the underlying graph will be directed and no reciprocity of the measurement is guaranteed. Moreover, given there are no self-measurements, the underlying graph has no self loops. It arises from def. 2 that each edge $e_k = e_{ij} = (v_i, v_j) \in \mathcal{E}, |\mathcal{E}| = m$ corresponds to a bearing measurement of agent j sensed by agent i $b_k = b_{ij}$. This measure belongs in the differential manifold $\mathcal{M}_k \subseteq \mathbb{S}^2$. Since there are m recorded measurements (one per each edge), the bearing measurement domain appears as $\hat{\mathcal{M}} = \prod_{k=1}^{m} \mathcal{M}_k \subseteq \mathbb{S}^{2m}$. Everything is now in order to define the core element in the construction of the bearing rigidity matrix.

Definition 3 (Bearing function) *Consider an n-agent formation modeled by a framework* $(\mathcal{G}, \mathcal{X})$ *in* $\hat{\mathcal{D}}$*. The map* $\mathbf{b}_\mathcal{G} : \hat{\mathcal{D}} \to \hat{\mathcal{M}}$*, which associates the formation configuration* $\mathcal{X} \in \hat{\mathcal{D}}$ *with the bearing measurements vector* $\mathbf{b}_\mathcal{G}(\mathcal{X}) = [\mathbf{b}_1^T \dots \mathbf{b}_m^T]^T \in \hat{\mathcal{M}}$ *is called bearing function.*

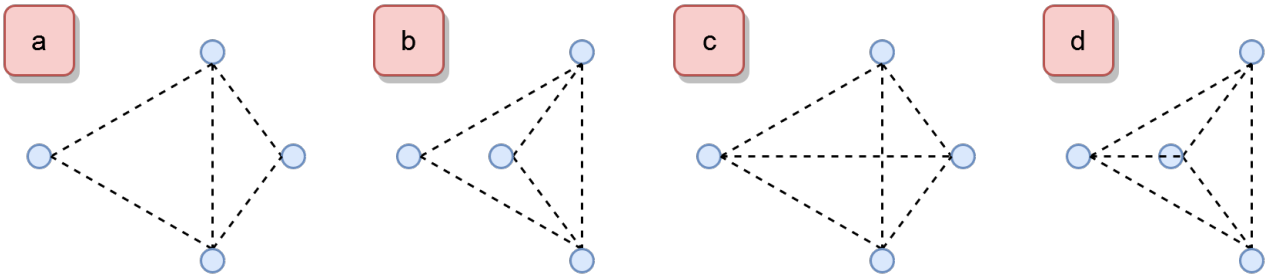

Figure 1.1: Bearing rigidity in a planar distance measurement scenario. See that framework **a** is equivalent to framework **b**, but they are not congruent, since their distances in the respective complete graph do not coincide (frameworks **c** and **d**). Frameworks **a** and **b** are LBR (since the jump between the BE formations requires going through a sequence of non-equivalent frameworks), while frameworks **c** and **d** are GBR.

Substantially, the bearing function defines the overall shape of the formation. It allows defining numerous properties for a framework:

Definition 4 (Bearing equivalence) *Two frameworks* $(\mathcal{G}, \mathcal{X})$ *and* $(\mathcal{G}\prime, \mathcal{X}')$ *are said to be bearing equivalent (BE) if their bearing functions coincide, namely if* $\mathbf{b}_{\mathcal{G}}(\mathcal{X}) = \mathbf{b}_{\mathcal{G}}(\mathcal{X}')$

Definition 5 (Bearing congruence) *Two frameworks* $(\mathcal{G}, \mathcal{X})$ *and* $(\mathcal{G}, \mathcal{X}')$ *are said to be bearing equivalent (BC) if their bearing functions coincide under their complete graph* $\mathcal{K}_{\mathcal{G}}$*, namely if* $\mathbf{b}_{\mathcal{K}}(\mathcal{X}) = \mathbf{b}_{\mathcal{K}}(\mathcal{X}')$

The complete graph $\mathcal{K}_{\mathcal{G}}$ is a graph in which an edge is present between each note. This means that a complete graph necessarily possesses $n(n-1)/2$ edges ($n(n-1)$ for a digraph) and corresponds to the optimal situation where each agent is able to sense one another. Note that requiring two bearing function to be equal for two different frameworks actually means that the swarm maintains the same overall shape, despite the fact it has moved in its manifold or some perturbation is present on its graph (bad connection or measurement). If one considers the preimage under the bearing function on $\mathcal{G}$ as the set $\mathcal{Q}(\mathcal{X})$ representing all the formations which are BE to $\mathcal{X}$, then the same can be said under the bearing function on $\mathcal{G}_{\mathcal{K}}$ which includes the formations which are BC to $\mathcal{X}$ as $\mathcal{C}(\mathcal{X})$. It is clear that BC is a stronger requirement than BE, so one has $\mathcal{C}(\mathcal{X}) \subseteq \mathcal{Q}(\mathcal{X})$. This allows to finally give a proper definition of (local) bearing rigidity.

Definition 6 (Local bearing rigidity) *A framework* $(\mathcal{G}, \mathcal{X})$ *is said to be locally bearing rigid (LBR) in* $\hat{\mathcal{D}}$ *if there exists a neighborhood* $\mathcal{U}(\mathcal{X}) \subseteq \hat{\mathcal{D}}$ *in which the formations which are BE are also BC. This means that* $\mathcal{C}(\mathcal{X}) \cap \mathcal{U}(\mathcal{X}) = \mathcal{Q}(\mathcal{X}) \cap \mathcal{U}(\mathcal{X})$

This definition can be intuitively interpreted as the fact that a locally rigid framework maintains the same overall shape even if only for minor perturbations to the framework, manifested through a different configuration $\mathcal{X}$.

Definition 7 (Global bearing rigidity) *A framework* $(\mathcal{G}, \mathcal{X})$ *is said to be globally bearing rigid (GBR) if it has* $\mathcal{C}(\mathcal{X}) = \mathcal{Q}(\mathcal{X})$ $\forall \mathcal{X} \in \hat{\mathcal{D}}$*, not limited to a neighborhood.*

This means that a GBR framework is guaranteed to maintain the same overall shape in the manifold irrespectively of the perturbations of the underlying configuration, and this is somehow justifiable if one considers that a complete graph implies complete reciprocal measurements between all the agents.

Dynamic frameworks

It is obvious that agents generally are able to move and change their configuration in time. This requires an extension of the concept of (static) rigidity to one of dynamic rigidity. A dynamic framework is nothing more than a sequence of static frameworks parametrized by a variable t representing time. From this point forward only dynamics framework are considered with $\mathcal{X} = \mathcal{X}(t) = \{\mathcal{X}_1(t) \dots \mathcal{X}_n(t)\}$ and the time notation will be dropped freely to improve readability.
The actuation on agent i causing the change in its configuration is named *variation* $\delta_\mathbf{i} \in \mathcal{I}_i$ (called agent variation domain), which defines the motion constraints for the agent in $\mathcal{D}_i$. The evolution of the configuration depends both on the configuration at an instant t and the actuation applied. This naturally gives rise to a function $f_i : \mathcal{D}_i \times \mathcal{I}_i \to \mathcal{D}_i$, which is supposed to be continuous and describes the evolution of the configuration over time:

$$f_i(\mathcal{X}(t), \delta_i) = \frac{d\mathcal{X}_i(t)}{dt}$$

As it has been done for the bearing measurements, it's possible to stack the variations characterizing each agent in a vector $\delta \in \hat{\mathcal{I}} = \prod_{i=1}^{n} \mathcal{I}_i$.
The impending question is the following: which are the condition under which a dynamic frameworks can deform (driven by variations) while maintaining its overall shape given by the relative bearings? In order to answer this question, one shall analyze the evolution of the bearing function by effect of the variations imparted on the formation. An very helpful tool comes in the form of the bearing rigidity matrix, which acts as a sort of geometric Jacobian for the bearing measurements:

Definition 8 (Bearing rigidity matrix(BRM)) *Given a dynamic framework $(\mathcal{G}, \mathcal{X}(t))$, the matrix $\mathbf{B}_\mathcal{G}(\mathcal{X}(t))$ satisfying*

$$\dot{b_\mathcal{G}}(\mathcal{X}(t)) = \frac{d}{dt} b_\mathcal{G}(\mathcal{X}(t)) = \mathbf{B}_\mathcal{G}(\mathcal{X}(t))\delta$$

is called bearing rigidity matrix.

This matrix directly links the variations to their effect on the bearing measurements. In particular $\mathbf{B}_\mathcal{G}(\mathcal{X}(t))$ is a function $\mathcal{I} \to \mathcal{M}$ and one can notice that its null space defines all the first order (referencing the Taylor expansion of the bearing function) variations which do not influence the bearing measurements, or in another way, all the actuation which can be applied to the swarm without modifying the cohesion of the formation, allowing to establish a sequence of BE frameworks. Such variations are called infinitesimal:

Definition 9 (Infinitesimal variation) *Given a dynamic framework $(\mathcal{G}, \mathcal{X})$, a variation $\delta \in \hat{\mathcal{I}}$ is infinitesimal if and only if $\delta \in ker(\mathbf{B}_\mathcal{G}(\mathcal{X}))$.*

A particular subset (it can be proven that $ker(\mathbf{B}_{\mathcal{G}}(\mathcal{X})) \subseteq ker(\mathbf{B}_{\mathcal{K}}(\mathcal{X}))$) of infinitesimal variations is given by *trivial variations*, which are basically infinitesimal variations applied to the complete graph of the original framework.

Defining the set of infinitesimal variations $\mathcal{S}_i := ker(\mathbf{B}_{\mathcal{G}}(\mathcal{X}))$ and the one of trivial variations $\mathcal{S}_t := ker(\mathbf{B}_{\mathcal{K}}(\mathcal{X}))$, it is possible to establish the notion of infinitesimal bearing rigidity.

Definition 10 (Infinitesimal bearing rigidity) *A dynamic framework $(\mathcal{G}, \mathcal{X}(t))$ is said to be infinitesimally bearing rigid (IBR) in $\hat{\mathcal{D}}$ if $ker(\mathbf{B}_{\mathcal{G}}(\mathcal{X})) = ker(\mathbf{B}_{\mathcal{K}}(\mathcal{X}))$ or equivalently, $\mathcal{S}_i = \mathcal{S}_t$. If this condition is not true, then it is infinitesimally bearing flexible (IBF).*

This means that even for a non-complete framework, if the dimension of the kernel of its bearing matrix is the same as the kernel of bearing matrix coming from the corresponding complete framework, it is guaranteed that there exist some shape-preserving actuation able to move the formation between different configurations.

Unified rigidity theory

Thanks to the work of [3], it is possible to expand the characterization of the bearing rigidity matrix irrespectively of the manifold in which the agents are supposed to belong, as long it is inside $SE(3)^n$. This approach not only gives a more rigorous and general description of rigidity theory, but also allows considering configurations which are not heterogeneous, in which each agent has different constraints pertaining to its translational and rotational degrees of freedom (DoF). Assume each agent i can vary in $\mathcal{D}_i$ with c_i^t translations DoFs and c_i^r rotational DoFs for a total of $c_i = c_i^t + c_i^r$ DoFs. Even though the movement of the agent could be limited, it can be described as a rigid body with attached local reference frame $\mathcal{F}_i$ originated in the CoM at O_i. At any time instant t the position of O_i in the world frame $\mathcal{F}_W$ is given by $p_i(t)$ while the orientation of $\mathcal{F}_i$ w.r.t. $\mathcal{F}_W$ is given by the rotation matrix $R_i(t)$. It is clear that if $c_i < 6$ the agent can change its pose only partially. In this setup, a local bearing measure of agent j by agent i along the edge k can be described as:

$$b_k(t) = b_{ij}(t) = R_i^T(t) s_{ij}(t) p_{ij}(t) = R_i^T(t) \hat{p_{ij}}(t) = R_i^T \frac{p_j(t) - p_i(t)}{||p_j(t) - p_i(t)||}$$

Since the framework presents m measurements (edges) and each one belongs to $\mathbb{S}^2$, the bearing domain can be embedded into $\mathbb{S}^{2m}$. By stacking all agent positions in $p(t) = [p_1^T(t) \dots p_n^T(t)]^T \in \mathbb{R}^{3n}$ bearing measurements can be easily recovered by exploiting the sensing graph $\mathcal{G}$, in particular its incidence matrix $E \in \mathbb{R}^{n \times m}$ can be expanded to the appropriate dimension by means of a Kronecker product giving $\hat{E} = E \otimes I_d \in \mathbb{R}^{dn \times dm}$:

$$b_{\mathcal{G}}^+(\mathcal{X}) = diag(s_{ij}\, R_i^T)\, \hat{E}\, p \in \mathbb{R}^{3m}$$

Finally, the variation domains can be lifted into $\delta^+ \in \mathbb{R}^{6n}$ by padding with zeros the allowed actuation, partitioned in $\delta_p \in \mathbb{R}^{3n}$ positional variations and $\delta_a \in \mathbb{R}^{3n}$ attitudinal variations:

$$\delta^+ = [\delta_p^{+T}\ \delta_a^{+T}]^T$$

The extended bearing rigidity matrix

These newfound elements allow the definition of an extended bearing rigidity matrix. Notice that the padding with zeros of the variations introduces null columns in the matrix, and that

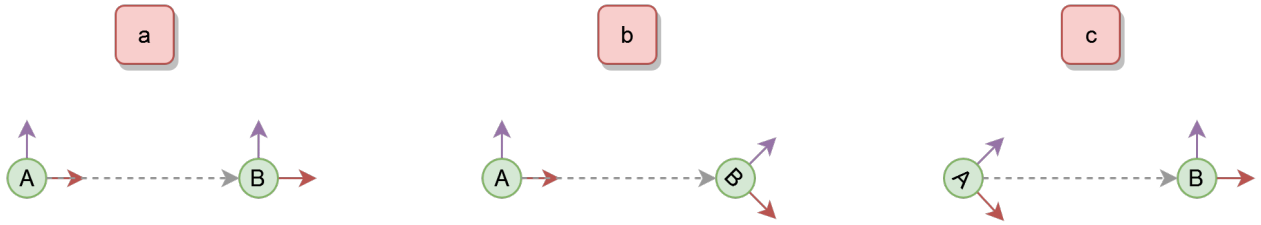

Figure 1.2: Dependence of the bearing measurement. Agent A has the same reading for both situation **a** and **b**, in which agent B frame has rotated. In situation **c** the reading is different since agent A's local frame has rotated.

such matrix can be partitioned in two column blocks, one referring to the effect on bearing variations of positional actuation and one of attitudinal actuation.

Definition 11 (Extended bearing rigidity matrix) *Given a dynamic framework* $(\mathcal{G}, \mathcal{X}(t))$, *the matrix* $\mathbf{B}_{\mathcal{G}}^{+}(\mathcal{X})$ *satisfying*

$$\dot{b_{\mathcal{G}}^{+}}(\mathcal{X}) = \frac{d}{dt} b_{\mathcal{G}}^{+}(\mathcal{X}) = \mathbf{B}_{\mathcal{G}}^{+}(\mathcal{X})\delta^{+}$$

is called extended bearing rigidity matrix

The dissertation in [3] also proves that is possible to find a particular partitioning of the bearing rigidity matrix, which also allows for a systematic approach in its composition:

$$\mathbf{B}_{\mathcal{G}}^{+}(\mathcal{X}(t)) = [D_p(t) U \hat{E}^T \; D_a(t) V \hat{E}_o^{\,T}] \in \mathbb{R}^{3m \times 6n} \tag{1.1}$$

Notice that the matrices $\hat{E}$ and $\hat{E}_o$ are time invariant if the framework is supposed to have constant sensing graph, and so are matrices U and V given the constraints on the agents don't vary during movement. In particular, $\hat{E}_o$ is the incidence matrix of the graph where only the outgoing edges are considered, meaning all the values which are not -1 are substituted by 0; this is due to the fact the local bearing measurements of agent j by agent i are not depending on variation the orientation of agent j, but only on the reciprocal position of agent i and j and orientation of agent i. See fig. 1.2 for clarification.

$U = diag(U_{ij}) \in \mathbb{R}^{3m \times 3m}$ is composed of m $U_{ij} \in \mathbb{R}^{3\times 3}$ blocks which describe the translational direction allowed for the bearing measurement b_{ij} while $V = diag(V_{ij}) \in \mathbb{R}^{3m \times 3m}$ has m blocks describing the allowed rotational direction of $\mathcal{F}_i$. The definition of these blocks rests entirely on the mutual characteristic of the two agents and their (eventual) constraints in the manifold and this is the main source of sparsity in the final matrix, given that they may add null columns and rows if some relative actuation is forbidden.

The only time-varying components of the matrices are the ones depending on the instantaneous condition of the formation, namely $D_p \in \mathbb{R}^{3m \times 3m}$ and $D_a \in \mathbb{R}^{3m \times 3m}$ which stem from the orthogonal projection of relative position and attitude:

$$D_p(t) = diag(s_{ij} \, R_i^T \, P(\hat{p_{ij}})) \qquad D_a(t) = -diag(R_i^T \, [\hat{p_{ij}}]_\times) \tag{1.2}$$

Where $P(x) = \mathbb{I}_3 - \frac{x}{||x||} \frac{x^T}{||x||}$ is the orthogonal projection operator such that $ker(P(x)) = \langle x \rangle$ and $P(x)y = y$ if $y \perp x$, while $[z]_\times$ is the skew-symmetric matrix generated from vector z which

allows depicting external products in $\mathbb{R}^3$ using matrix multiplication: $z \times v = [z]_\times v$

The sets of infinitesimal and trivial variations considered beforehand can be lifted into $\mathbb{R}^{6n}$ as well yet maintaining the same cardinality ($|\mathcal{S}_i^+| = |\mathcal{S}_i| = q_i$ and $|\mathcal{S}_t^+| = |\mathcal{S}_t| = q_t$). This implies that necessarily the kernel must expand in order to accommodate for the greater number of zero columns of the bearing rigidity matrix. The elements of this portion of the kernel are named *virtual variations*, symbolized as $\mathcal{S}_v$ with $|\mathcal{S}_v| = q_v$, and describe substantially the movements which are constrained for each agent in the manifold. Therefore, for an extended bearing rigidity matrix it holds:

$$ker(B_{\mathcal{G}}^+(\mathcal{X})) = S_i^+ \oplus S_v^+ \qquad ker(B_{\mathcal{K}}^+(\mathcal{X})) = S_t^+ \oplus S_v^+$$

This fact is vital since it allows establishing a sufficient and necessary condition for infinitesimally bearing rigidity:

Theorem 1 (Rank condition for IBR) *Given a noncollinear dynamic framework $(\mathcal{G}, \mathcal{X}(t))$ in a generic differential manifold $\hat{\mathcal{D}}$, it is IBR if and only if $rank(B_{\mathcal{G}}^+(\mathcal{X})) = rank(B_{\mathcal{K}}^+(\mathcal{X}))$*

Proof 1 *Given that $n \leq m$, the lesser dimension of the bearing matrix is the $6n$ columns. This means $rank(B_{\mathcal{G}}^+(\mathcal{X})) = 6n - |ker(B_{\mathcal{G}}^+(\mathcal{X}))| = 6n - (|S_i^+| + |S_v^+|) = 6n - (q_v + q_i)$ and similarly $rank(B_{\mathcal{K}}^+(\mathcal{X})) = 6n - (q_v + q_t)$. So for $q_i = q_t$ the two ranks coincide. Since as seen previously $ker(\mathbf{B}_{\mathcal{G}}(\mathcal{X})) \subseteq ker(\mathbf{B}_{\mathcal{K}}(\mathcal{X}))$, this implies that $q_i \leq q_t$ and consequently $q_i = q_t \iff ker(B_{\mathcal{G}}^+(\mathcal{X})) = ker(B_{\mathcal{K}}^+(\mathcal{X})) \iff$ the framework is IBR.*

This result is paramount. Through a simple check on the rank of the bearing rigidity matrix, one can immediately characterize if the framework is IBR. This is particularly important given the following theorem:

Theorem 2 (IBR, GBR and BR relation) *Given a noncollinear dynamic framework $\mathcal{J} = (\mathcal{G}, \mathcal{X}(t))$ in a generic differential manifold $\hat{\mathcal{D}}$, it holds for any t:*

- *$\mathcal{J}$ is IBR if and only if it is BR*
- *$\mathcal{J}$ is IBR if it is GBR*

This means that an GBR framework implies an IBR framework, and that IBR and BR are equivalent conditions, meaning that the rank condition for IBR translated into a rank condition for GR, which guarantees that for limited motions the formation shape will be maintained.

1.2 The experimental setup

All the work presented is carried out via numerical simulations on Matlab.
The main case studies are given by homogenous and non-homogenous frameworks in the manifold $\hat{\mathcal{D}} = SE(3)$. The agents considered are of two possible types:

- UGV (unmanned ground vehicle) which is constrained to move on the x-y plane and can only rotate around its z axis. This means $c_i^t = 2$ and $c_i^r = 1$, with $c_i = 3$.

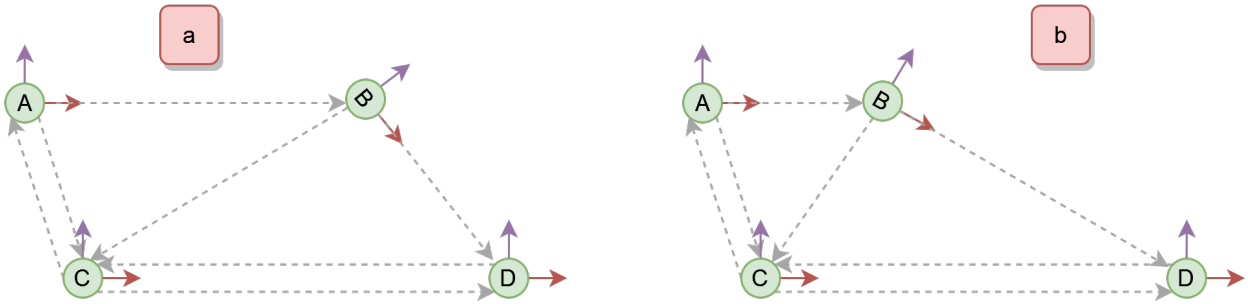

Figure 1.3: Note that the two frameworks are IBR (the bearing measurements from and to node B are unchanged in both **a** and **b** despite its movement in the manifold) but not GBR, since under the complete graph the bearings would be no longer the same.

- UAV (unmanned aerial vehicle) modeled as an under-actuated quad rotor having only control on its yaw orientation (assumed parallel to the z-axis and its position. For this it holds $c_i^t = 3$ and $c_i^r = 1$, with $c_i = 4$.

Sensing is considered as coming from bearing measurements estimated from omnidirectional cameras, removing the need to consider connected only agents which remain within the FOV of one another, and consisting on a local measurement in the agent frame $\mathcal{F}_i$: the underlying graph is therefore directed. The bearing measurements are simulated from positions and orientations of the swarm in the absolute frame $\mathcal{F}_W$ and uncertainty of measure is modeled by the addition of Gaussian noise with zero mean and variance $\Sigma = \sigma \cdot \mathbb{1}_3$. From now on, all `monospaced` text is referring to variables present in the source code.
The source code is accessible at [`https://gitlab.com/xomcar/unipd-rigidity-thesis`].

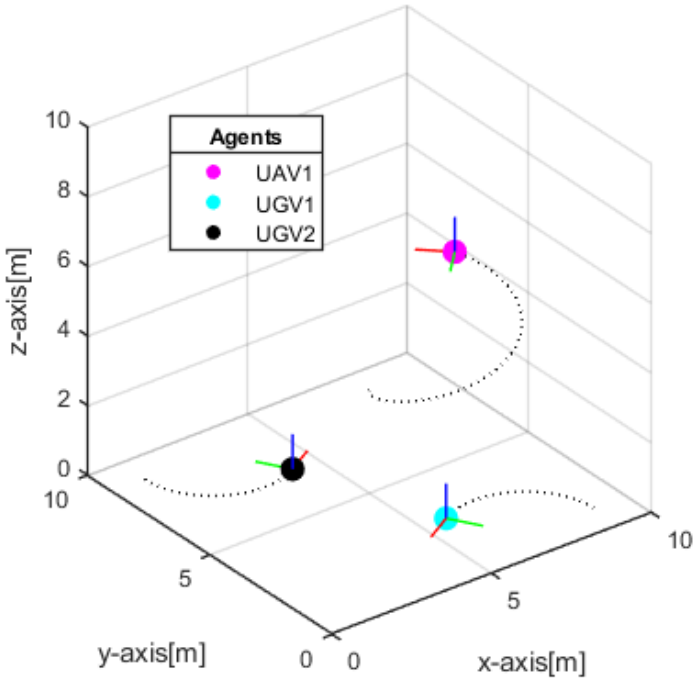

Figure 1.4: This is the simulation space considered in Matlab. Each agent has its own position and frame. UGV are constrained to move in the z = 0 plane, while UAVs can move freely in the 3D space. Rotations of frames is allowed only around the frame axis parallel to the absolute z-axis

Chapter 2

Trials

2.1 Building the bearing rigidity matrix

In order to build the bearing rigidity matrix following the structure showed in eq.1.1, it is necessary to define a proper framework which will be characterized by it.
The matrix $\texttt{SWARM} \in \mathbb{R}^{5\times n}$ represents the formation parameters, in which each column is referring to a single agent (for a total of n).

$$\texttt{SWARM} = \begin{bmatrix} & \dots & & & \\ \texttt{type} & p_x^W & p_y^W & p_z^W & \theta_z^W \\ & \dots & & & \end{bmatrix}^T \tag{2.1}$$

The label `type` defines whether the column is describing a UAV (value 2) or UGV (value 1). $[p_x^W \ p_y^W \ p_z^W]^T = \texttt{pos}^W \in \mathbb{R}^3$ is the agent position (in meters) in referred to its CoM in $\mathcal{F}_W$. Since both UAVs and UGVs have only one DoF in rotation around z (vertical axis of $\mathcal{F}_W$) only the rotation amount around z, $\theta_z^W \in [0, 2\pi)$, is specified.

In order to represent the graph edge (measurements direction), two vectors in $\mathbb{R}^m$ are established representing the source (`sourceNodes`) and target (`targetNodes`) of each measure as an index $\in \{1...n\}$ referring to the column in matrix 2.1. Since there is also the need to discriminate the nature of the measurement when populating the matrices U_{ij} and V_{ij}, the weights of the edges (`edgeWeights`) are used as an indication of this characteristic, by placing them in a $\mathbb{R}^m$ vector with value 1, 2, 3, 4 for UGV $\rightarrow$ UGV, UGV $\rightarrow$ UAV, UAV $\rightarrow$ UGV, UAV $\rightarrow$ UAV respectively. Reference to fig. 2.1 for a graphical description of the graphs variables.

Now that the swarm is properly defined in all its characteristics, iterating through each edge of the graph simulates the measurement. For each edge k (going from agent i to agent j) are computed:

- $\texttt{worldLink} = \texttt{pos}_j^W - \texttt{pos}_i^W = p_{ij} \in \mathbb{R}^3$, which is the vector (in $\mathcal{F}_W$) linking the two agents
- $\texttt{dist} = ||p_{ij}|| = s_{ij}^{-1} \in \mathbb{R}$, which is the distance between the agents
- $\texttt{worldBearing} = \hat{p_{ij}} = p_{ij}s_{ij} \in \mathbb{S}^2$, which is the bearing measurement in $\mathcal{F}_W$

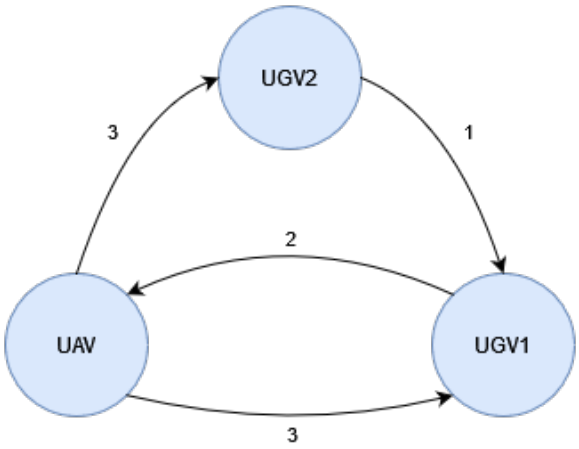

Figure 2.1: Example for clarification of graph definition. Corresponding vectors of nodes are `sourceNodes` $= [1\ 1\ 2\ 3]^T$, `targetNodes` $= [2\ 3\ 1\ 2]^T$, `weightEdges` $= [3\ 3\ 2\ 1]^T$. The labels of the nodes are [`UAV`, `UGV1`, `UGV2`]^T.

- `localBearing` $= R_i^T \hat{p_{ij}} \in \mathbb{S}^2$, which is the local bearing measurement in $\mathcal{F}_i$. $R_i = R_i^W \in SO(3)$ is the orientation of $\mathcal{F}_i$ w.r.t. $\mathcal{F}_W$

It's now possible to populate the elements that will compose the bearing rigidity matrix using the equation 1.1. In particular, for the formation of the matrices $U \in \mathbb{R}^{3m\times 3m}$ and $V \in \mathbb{R}^{3m\times 3m}$, a block diagonal matrix is formed in which each block $U_{ij} \in \mathbb{R}^{3\times 3}$ and $V_{ij} \in \mathbb{R}^{3\times 3}$ are picked accordingly to the nature of the agents i and j from the pool described in table 2.1.
The incidence matrices $E \in \mathbb{R}^{n\times m}$ and $E_o \in \mathbb{R}^{n\times m}$ are computed from the graph and expanded

Node i	Node j	U_{ij}	V_{ij}	Bearing type	Bearing number
UGV	UGV	$\begin{matrix}1&0&0\\0&1&0\\0&0&0\end{matrix}$	$\begin{matrix}0&0&0\\0&0&0\\0&0&1\end{matrix}$	UGV → UGV	1
UGV	UAV	$\begin{matrix}1&0&0\\0&1&0\\0&0&1\end{matrix}$	$\begin{matrix}0&0&0\\0&0&0\\0&0&1\end{matrix}$	UGV → UAV	2
UAV	UGV	$\begin{matrix}1&0&0\\0&1&0\\0&0&1\end{matrix}$	$\begin{matrix}0&0&0\\0&0&0\\0&0&1\end{matrix}$	UAV → UGV	3
UAV	UAV	$\begin{matrix}1&0&0\\0&1&0\\0&0&1\end{matrix}$	$\begin{matrix}0&0&0\\0&0&0\\0&0&1\end{matrix}$	UAV → UAV	4

Table 2.1: The blocks U_{ij} and V_{ij} are chosen from this table.

into $\hat{E} \in \mathbb{R}^{3n\times 3m}$ and $\hat{E}_o \in \mathbb{R}^{3n\times 3m}$ using the Kronecker product.
Matrices $D_p \in \mathbb{R}^{3\times 3}$ and $D_a \in \mathbb{R}^{3\times 3}$ are computed accordingly to equation 1.2. Note that despite only admitting local measurements, the equations use global information pertaining to R_i. This is an admissible supposition, since there are numerous algorithms which allow the estimation of such value in the literature [10].

In order to check whether the resulting BRM $B \in \mathbb{R}^{3m \times 6n}$ is valid, one has to check the rank of the matrix itself and the basis of the kernel in order to verify that all the infinitesimal variations are accounted for. The procedure will be further exemplified in chapter 3.

2.2 Analyzing the bearing rigidity matrix

The BRM is a big and sparse matrix, therefore trying to recognize pattern or variations in it is no easy feat.
First, since BRM is not (for the most cases) a square matrix, in order to characterize it one can use its singular values, corresponding to the square roots of the eigenvalues of the symmetric bearing rigidity matrix (SBRM) $\mathcal{S}_\mathcal{G} = B_\mathcal{G}^T B_\mathcal{G} \in \mathbb{R}^{6n \times 6n}$. For the sake of simplicity, eigenvalues will be considered in the following.
As an example, consider two SBRMs, $B_a \in \mathbb{R}^{18\ \times 18}$ and $B_b \in \mathbb{R}^{18\ \times 18}$ and their eigenvalues in ascending order, $\Lambda_a = [\lambda_a^1 \dots \lambda_a^{18}]$ and $\Lambda_b = [\lambda_b^1 \dots \lambda_b^{18}]$. If $rank(ker(B_a)) = rank(ker(B_b)) = 8$, then the first non-null eigenvalues will be λ_a^9 and λ_b^9. Whichever of the two is closer to zero indicates which one of the BRM is closer to become IBF.
Remembering that

$$\dot{b}_\mathcal{G} = B_\mathcal{G}\, \delta$$

and assuming δ to be the actual control motions imparted to the swarm agents in terms of linear and angular velocities which causes a bearing measurement change of $\dot{b}_\mathcal{G}$, if one considers the squared norm of the latter as a quantifier of how much the measurement changes it obtains:

$$||\dot{b}_\mathcal{G}||^2 = \delta^T\, B_\mathcal{G}^T B_\mathcal{G}\, \delta = \mathcal{S}_\mathcal{G}\, ||\delta||^2$$

through which the SBRM can be seen as acting as a sort of gain of the control effort into the bearing changes. It is therefore desirable to describe the "magnitude" of the SBRM, for example using the squared Frobenious norm $||B_\mathcal{G}||_F^2$, representing the trace of the SBRM or equivalently the sum of all its eigenvalues.

In addition, by noticing the partitioning of the BRM into two column blocks given by eq. 1.1, one can think of rearranging the columns of the matrix in order to compress the information pertaining the same agent instead of the one pertaining the same actuation. In particular, considering the motion of each agent i is described as two triplets $v_i = [\dot{p}_x\ \dot{p}_y\ \dot{p}_z]^T$ and $\omega_i = [\dot{\theta}_x\ \dot{\theta}_y\ \dot{\theta}_z]^T$, one can permutate the columns as seen in fig. 2.4 in order to highlight what effect the motion of a single agent has on the various bearing measurements. In particular, the diagonal blocks describe the effect the motion of the agent has in the bearing measurements stemming from itself. Analyzing the eigenvalues of these blocks could help in better understanding the dynamics of the matrix when a single agent is in motion. The permutated BRM will be referred as PBRM.

Observe fig. 2.2: each block B_{ij} encodes how the actuation of agent j modifies the bearing measurement coming from agent j. In particular, in the case of the diagonal blocks, it contains the effect that moving an agent has on its very bearing measurements. By examining the non-null singular values of the diagonal block B_{ii} while moving agent i in the manifold, one can observe the configurations in which the bearing is more dependent on the motion of agent i. This may reveal some information regarding eventual symmetries.

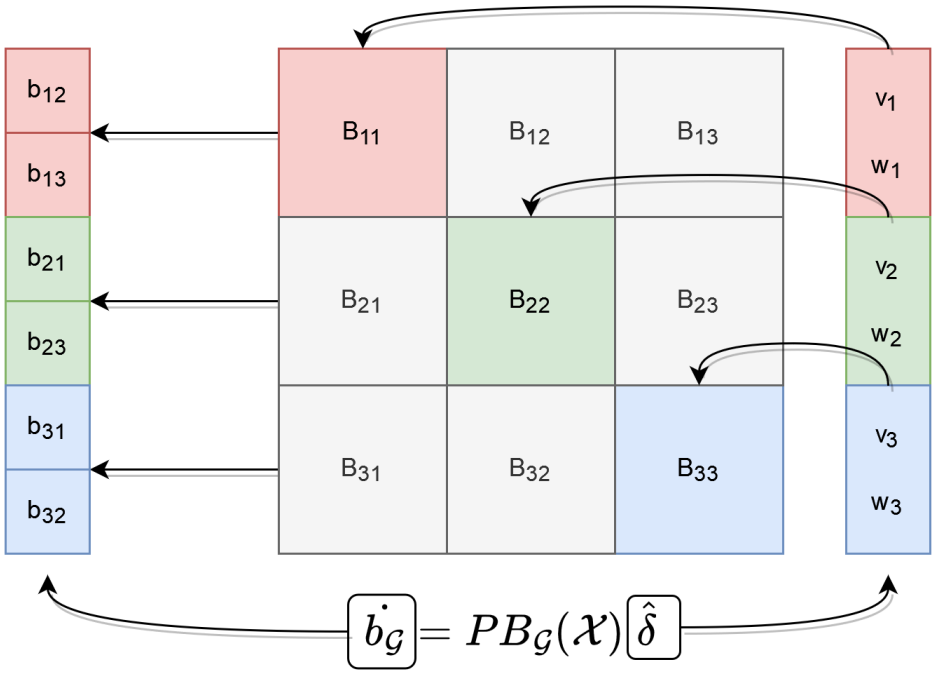

Figure 2.2: Schematic description of the newfound partition of the PBRM. $\hat{\delta}$ is the shuffled version of the input vector, no longer partitioned by linear and rotational inputs, but by agent. In a nutshell, block B_{ij} encodes how the movement of agent j conditions the reading of agent i. Therefore, the diagonal blocks encode how each agent movement conditions its readings. In particular, given the sparsity of the non-diagonal elements, this can be considered a good approximation of the BRM, given that also the minimum between the eigenvalues of the diagonal blocks more or less coincides with that of the original BRM.

2.3 Simulation procedure

First, a series of simulations are carried out in different configurations in order to confirm the theoretical premises and correct implementation of the code:

1. A noiseless BRM is computed for the current configuration on a complete and incomplete graph (removed edges are picked randomly)

2. Rank condition (based on considerations on the formation) is checked on BRM to establish IBR

3. The kernel of the BRM is studied in order to verify the presence of the trivial variations accounted in (2)

4. The same framework is then perturbed in a `SCALED` (distances) version and in one with randomly `MORPHED` positions

5. Eigenvalues of SBRM are computed for each framework (`NORMAL`, `SCALED` and `MORPHED`) and compared

6. Frobenious norms of each SBRM is computed for each framework (`NORMAL`, `SCALED` and `MORPHED`) and compared

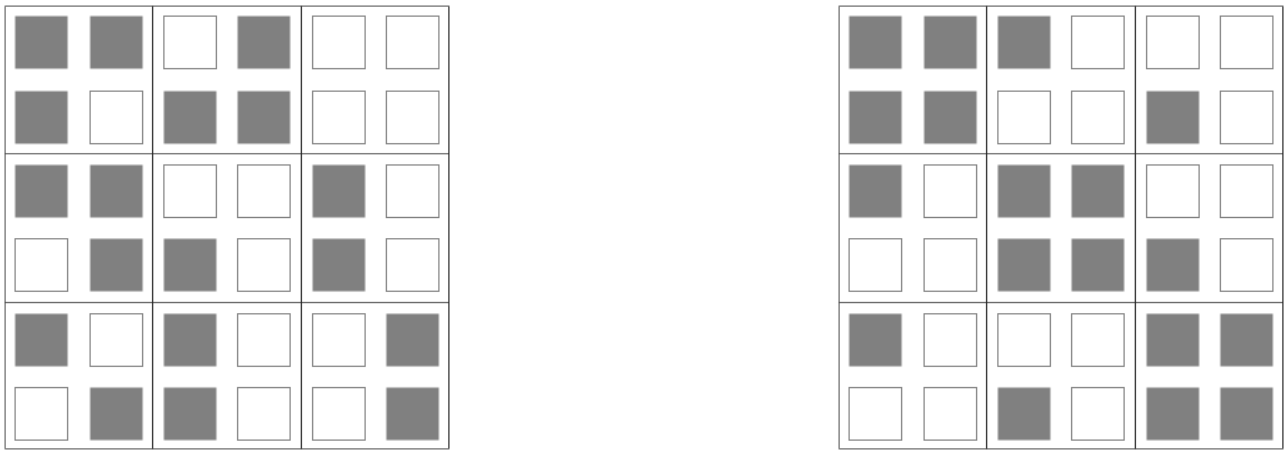

Figure 2.3: Example of column permutation effect on sparsity on a BRM $\in \mathbb{R}^{18\times18}$. Each block is in $\mathbb{R}^{6\times6}$. Left: original BRM matrix. Right: permutated one. Gray elements represent non-null blocks, white elements are fully zero blocks. Notice how the non-null gray blocks on diagonal encode most of the information.

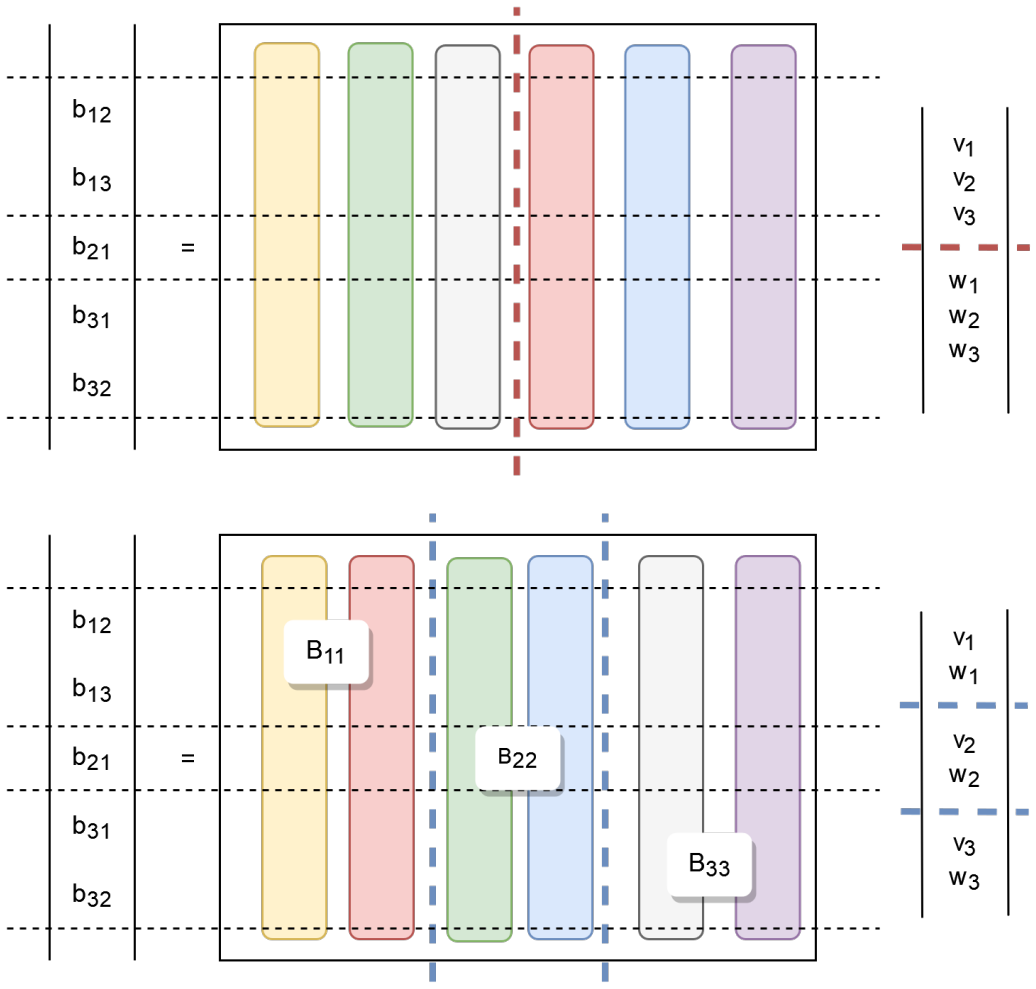

Figure 2.4: Example of column permutation on a BRM $\in \mathbb{R}^{15\times18}$.
Upper: original BRM matrix. Lower: permutated one. Notice how the blocks on the diagonal characterize the effect the motion of each node has in its own bearing measurements

Then the effect of noisy measurements is considered for different configurations:

1. A noisy BRM is computed for the current configuration on a complete and incomplete graph (removed edges are picked randomly) with noise on 1, 2, 4 or all measurements.
2. Rank condition (based on considerations on the formation) is checked on BRM to establish IBR
3. Eigenvalues of SBRM are computed and compared
4. Frobenious norms of each SBRM is computed and compared

Chapter 3

Results

3.1 Verification of assumptions

Effectiveness of algorithm: heterogeneous 5 agents fleet

The first formation considered consists of 4 UGVs and 1 UAV disposed symmetrically around $[3, 3, 0]^T$ with radius 0.5 m. Fig 3.1 gives a pictorial representation of the formation. The virtual variations are $n \cdot 2+1 = 11$ (each agent has 2 rotations blocked plus the z movement is forbidden for the UGVs) and the trivial variations are 4: scaling, global movement along x, along y and coordinated rotation. This means that the expected dimension of the kernel is $11 + 4 = 15$. Since $n \cdot 6 = 30$, the expected $rank(B) = 30 - 15 = 15$. To further confirm the correctness, for each of these movements the linear dependency with the kernel of the BRM: all the 4 trivial variations must be linearly dependent. In tab. 3.1 one can observe the gathered data which confirms that the incomplete frameworks can be nonetheless IBR. For this configuration, the number of edges for the complete case is $n \cdot (n - 1) = 20$. In fig 3.2 the eigenvalues of the matrix can be seen.

	$rank(B)$	$\lambda_{16}(B^TB)$	$\|\|B^TB\|\|_F^2$	Trivial set lin. dep.
Complete	15	0.0707	29.3183	Yes
-4 edges	15	0.0397	26.8871	Yes
-7 edges	15	0.0229	22.3331	Yes
-10 edges	13	≈ 0	20.1171	Yes

Table 3.1: Simulation data for heterogeneous fleet of 5 agents. By removing 10 edges out of 20 the formation is no longer IBR. Notice how the more the formations becomes flexible, the more the smallest eigenvalue approaches zero and the norm of the matrix diminishes. The trivial variations remain included in the kernel even after the framework has become IBF, but this is expected since two more infinitesimal variations have entered the kernel due to the fact that the rank of B has dropped.

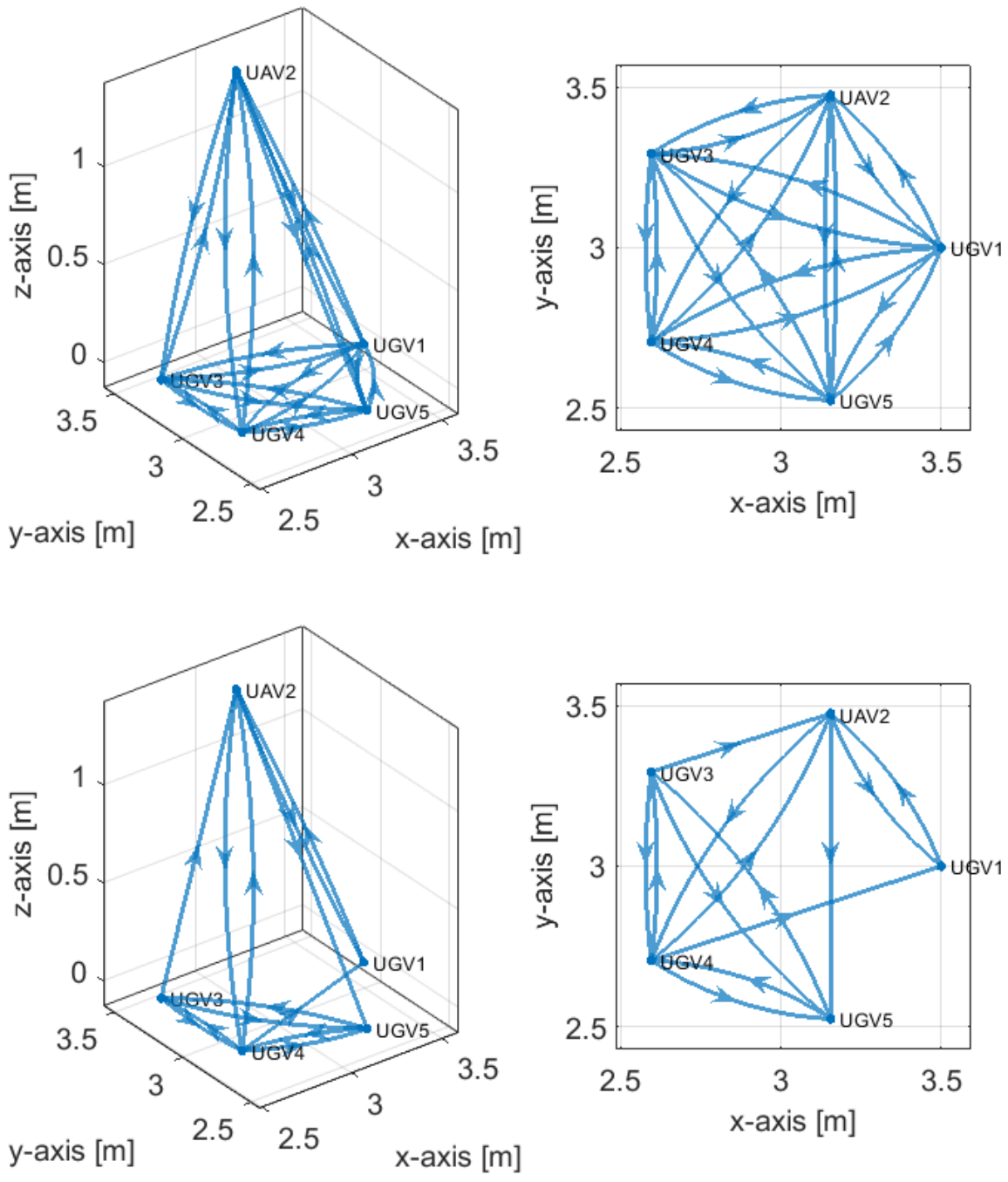

Figure 3.1: Spatial framework reference for the formation.
Upper: complete graph. Lower: incomplete graph (-7 edges). Even though the graph is not complete (UGV1 and UGV5 do not sense each other!) the IBR condition remains satisfied.

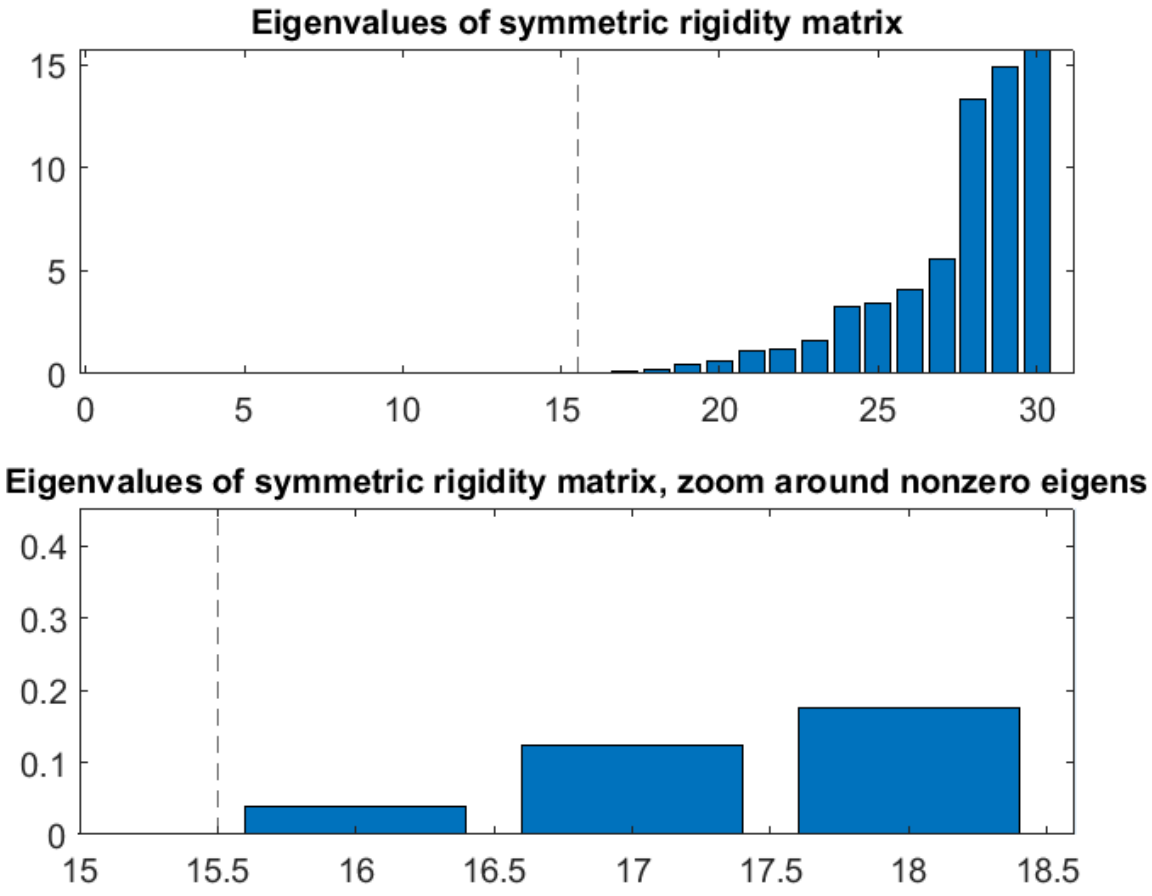

Figure 3.2: Heterogeneous 5 agents swarm, eigenvalues of the complete graph formation. The dotted line represents the first expected non-zero eigenvalue according to the rank requirements for IBR for the considered configuration.

Scalability of algorithm: homogeneous 20 UAVs fleet

For the sake of testing the robustness of the code, a formation comprises 20 UAVs is considered. Disposed symmetrically around $[3, 3, 0]^T$ with radius 0.5 m. The virtual variations are $n \cdot 2 = 40$ (each agent has 2 rotations blocked) and the trivial variations are 5: scaling, global movement along x, along y, along z and coordinated rotation. This means that the expected dimension of the kernel is $40 + 5 = 45$. Since $n \cdot 6 = 120$, the expected $rank(B) = 120 - 45 = 75$. The number of edges is $n \cdot (n - 1) = 380$. Table 3.2 illustrates the results for this fleet.

	$rank(B)$	$\lambda_{46}(B^T B)$	$\|\|B^T B\|\|_F^2$	Trivial set lin. dep.
Complete	75	5.4240	833.7111	Yes
-20 edges	75	5.3870	804.4807	Yes
-50 edges	75	4.8490	737.6025	Yes
-100 edges	75	4.0340	685.3442	Yes
-200 edges	75	2.0933	464.5554	Yes
-300 edges	75	0.2641	155.5196	Yes
-350 edges	60	≈ 0	64.4952	Yes

Table 3.2: Simulation data for the 20 UAVs swarm. Notice how the percentage of the edges lost reflects pretty accurately the percentage loss in the norm of the matrix. For example, $360/380 = 0.9474$ and $804.48/833.71 = 0.9649$, while $30/380 = 0.0789$ and $64.49/833.71 = 0.0774$.

Robustness to perturbation of the configuration: homogeneous 4 UGVs fleet

This formation is composed of 6 UGVs disposed symmetrically around $[3, 3, 0]^T$ with radius 0.5 m. This time analysis is carried out to compare the modifications applied to the configuration. Expected kernel has dimension $3 \cdot n + 4 = 16$ and therefore the required $rank(B) = 24 - 16 = 8$. This time the formation is first scaled and then morphed around the plane (see fig. 3.3 for a pictorial reference). In fig. 3.4 one can observe the eigenvalues comparison for the considered cases.

	$rank(B)$	$\lambda_{17}(B^TB)$	$\|\|B^TB\|\|_F^2$
Original	8	1.4384	7.21
Original -2 edges	8	0.5780	6.48
Original -4 edges	8	0.1565	5.83
Original -6 edges	6	≈ 0	5.29
Scaled	8	0.9222	5.46
Scaled -2 edges	8	0.4433	4.92
Scaled -4 edges	8	0.0807	4.42
Scaled -6 edges	6	≈ 0	3.97
Morphed	8	0.0051	3.55
Morphed -2 edges	8	0.0036	3.24
Morphed -4 edges	8	0.0006	2.89
Morphed -6 edges	6	≈ 0	2.51

Table 3.3: Simulation data for the 3 different UGVs configurations. It is possible to observe that both symmetry and distance play an important role on the rigidity of the framework: the minimal eigenvalue for the scaled formation is lower than the original one, so it's clear the bearings encode distance information. This is intuitive since for the same motion at different distances, the angle spanned between the two bearings is proportional to the distance itself (i.e. distant moving agents have less effects on bearing than closer ones). As for symmetry, we can observe that the morphed framework is very close to the IBF condition even in the scenario with the complete graph. A symmetric configuration is guaranteed to be noncollinear, so it is only natural that a randomly morphed configuration would have a lower performance w.r.t. rigidity, given it can happen that the disposition of the agents gets closer to an aligned one. This aspect will be further investigated in the following subsection 3.1.

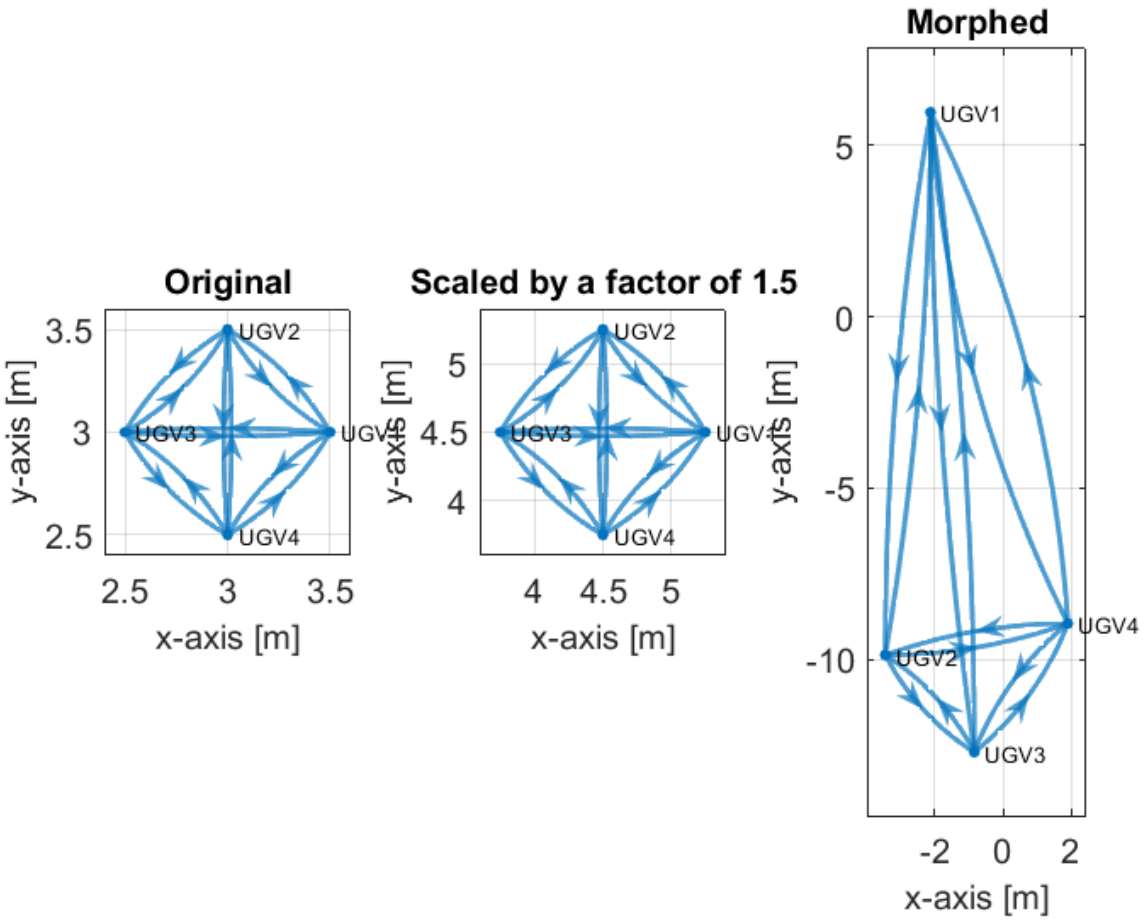

Figure 3.3: Framework reference for the perturbed UGV formations under complete graph. Note that the morphed configuration gives a condition which is less rigidity, given that the bearing readings of agent 3 are very close to one another.

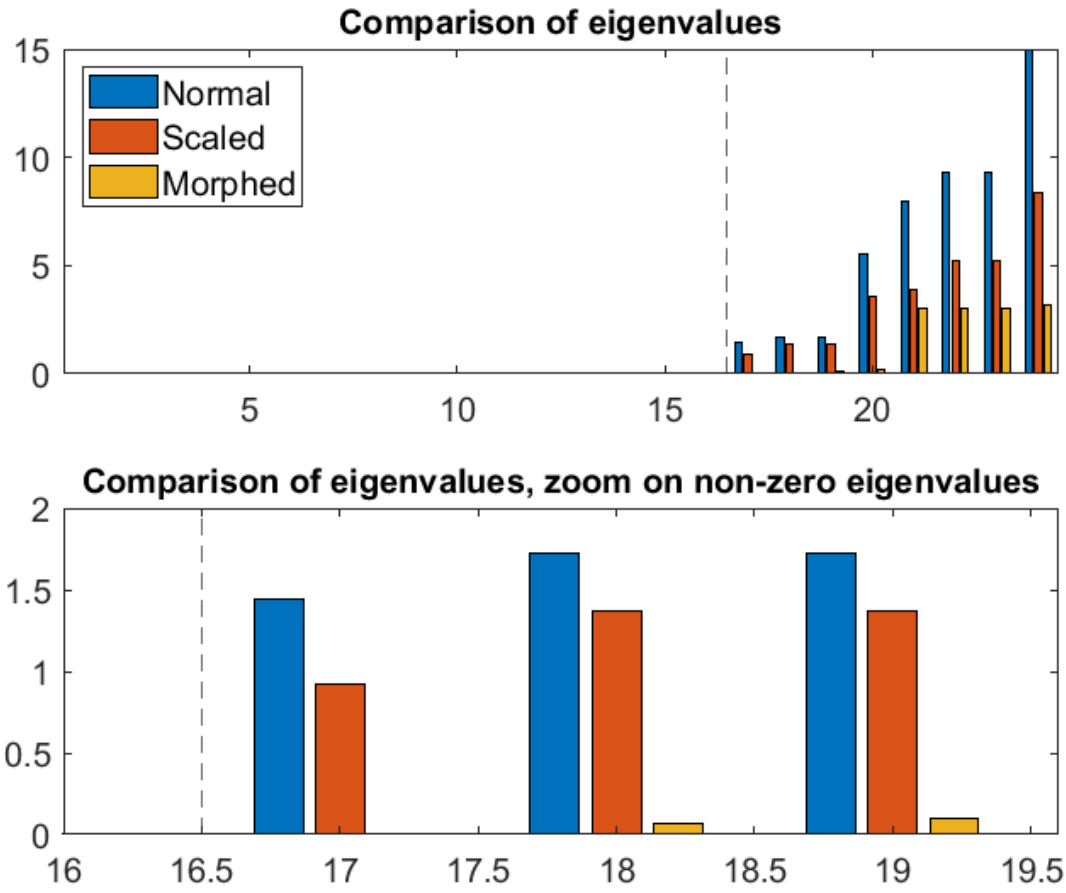

Figure 3.4: Comparison of the eigenvalues for the 3 UGVs configurations. λ_{17} for the morphed case is not zero but seems so due to scale. Evidently, the morphed framework is very close to become IBF, having lost symmetry and possibly approaching a collinear scenario. From this graph it is possible to observe that distance plays an important role in the rigidity of the formation.

Rigidity and collinearity: homogenous 3 UAVs fleet

In order to highlight the effect of collinearity on the BRM, a UAV formation is assembled such that the agents are placed almost in line with one another. The formation considered can be seen in fig. 3.5. The expected $rank(B) = 5 = 6 * 3 - 13$ and the requirement is satisfied, but looking at the eigenvalues one can see that the framework is still rigid by a miracle: $\lambda_{14} = 0.0008$, while $\lambda_{15} = 1.345$, almost 4 magnitudes of difference. In fact, by moving agent 1 from x = 0.98 to x = 1 the rank drops and $\lambda_{14} = 4 \cdot 10^{-14}$! The effect of the analysis of the eigenvalues is clear, even more so than the rank itself which can be misleading in correctly evaluating the rigidity of the formation.

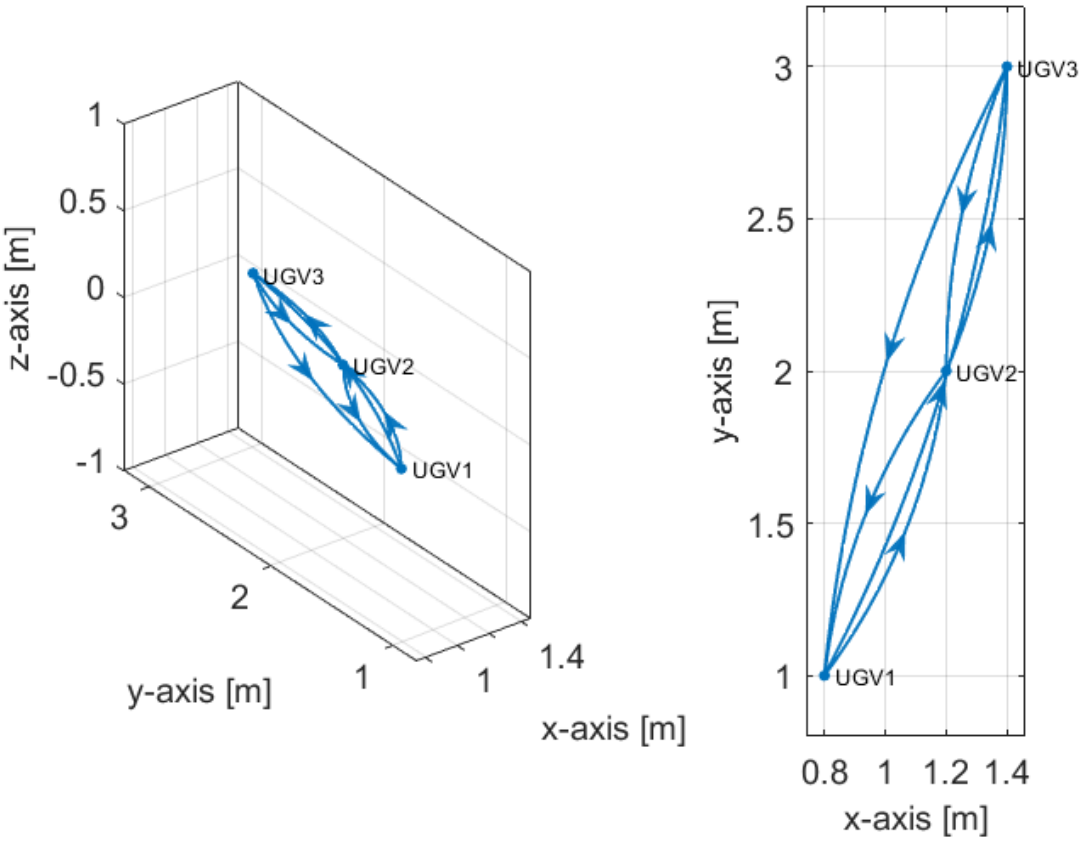

Figure 3.5: It is pretty noticeable that the configuration is close to collinearity. This means that for example UAV1 has two basically identical bearing for UAV2 and UAV3, which leads to an informative deficit that subtracts rigidity to the framework.

3.2 Effect of noise

The effect of noisy readings is simulated during the computation of the BRM matrix by addition of a vector $n \in \mathbb{R}^3$ picked randomly from a normal multivariate distribution with mean 0 and variable variance. The effect of such addition to the bearing measurement is quantified by calculating the angle displacement between the original bearing (v_1) and the noisy one (v_2),

namely $\theta_{err} = \texttt{atan2d}(||v_1 \times v_2||\ ,\ v_1 \cdot v_2)$, where atan2d is the four-quadrant inverse tangent. Noise is added in the local bearing measurements as follows:

$$b_{err} = \mathcal{N}(\mu, \Sigma)$$

$$\texttt{localBearing} = \texttt{localBearing} + b_{err}$$

$$\texttt{localBearingMeasurement} = \frac{\texttt{localBearing}}{||\texttt{localBearing}||}$$

$$\texttt{globalBearingMeasurement} = R_i\ \texttt{localBearingMeasurement}$$

Homogenous 4 agents fleet UAV, planar disposition

The first formation consists of 6 UAVs with complete graph disposed symmetrically around $[3, 3, 1]^T$. As a first, all UAVs are placed at the same height $z = 1$. Having 5 trivial motions and $2 * n = 8$ virtual motions, the framework should account for $dim(ker(BRM)) = 13$, which is in fact confirmed from the BRM (B_0) of the non-noisy formation. Trivial motions are also checked and all of them (coordinated rotation, translation and scaling) belong to the kernel. Now, a single measurement is tainted with error, in particular $b_1 = b_{1\to2}$, with a bearing error of 8.13 [deg]. Considering that the formation is placed along a square, the bearings fluctuate between 90 and 45 degrees, meaning this error can be as high as 18% of the true value.
Analysis of the BRM coming from this configuration (B_1) signals that the matrix has raised in rank! In particular, $dim(ker(B_1)) = 11 < dim(ker(B_0))$. This is quite inexplicable since at most one should expect the rank of the matrix to drop with the loss of rigidity induced by the error. By lowering the variance to $\sigma = 0.00001$ the bearing error is now at 0.0014 [deg], around 0.003%, which one should expect to be non-impactful at all. However, the noisy matrix still gives the same rank at $dim(ker(BRM)) = 11$. By analyzing the eigenvalues, it shows that $\lambda_{13} = 2.8910^{-10}$, which can be safely considered as a zero eigenvalue given that $\lambda_{14} = 0.7996$ is 9 magnitudes higher: this seem to be a numeric problem given by the Matlab routine which computes the rank of matrix. Therefore, for the next considerations instead of checking the rank value given by the Matlab routine, we will consider the dimensional discrepancy between the two eigenvalues around the required rank condition. Table 3.4 gives an outlook on the outcome of the simulations. Error ratio is computed considering the average error of all the measurements and the maximum magnitude of the bearing (which for a planar 4 agents configuration is 45 [deg]).

In order to further highlight the influence of the error on the BRM, a morphed, non-symmetric configuration has been considered. Starting from a less rigid BRM, table 3.5 shows the evolution of the error, which confirms that the initial configuration of the swarm plays an important role on the effect of the error.

Finally, it is interesting to observe how the noise evolves for a swarm disposition scaled by a factor of 1.5. The result sits in an in-between the two previous conditions (table 3.6.

Variance	# Noisy edges	Average error ratio	λ_{14}	λ_{13}	$\lambda_{13}/\lambda_{14}$	$\|\|B\|\|_F^2$
-	0	-	1.298	$10^{-16} \approx 0$	0%	26.936
0.001	1	0.13%	1.297	$1.95 \cdot 10^{-6}$	0.0002%	26.936
	2	0.19%	1.298	$1.28 \cdot 10^{-6}$	0.0001%	26.937
	4	0.19%	1.297	$6.25 \cdot 10^{-6}$	0.0005%	26.931
	12	0.14%	1.298	$7.64 \cdot 10^{-6}$	0.0006%	26.931
0.03	1	9.90%	1.270	0.0017	0.13%	26.919
	2	5.83%	1.305	0.0014	0.08%	26.967
	4	5.77%	1.256	0.0056	0.44%	26.792
	12	4.23%	1.312	0.0065	0.50%	26.878
0.06	1	19.55%	1.238	0.0069	0.55%	26.884
	2	11.69%	1.310	0.0047	0.34%	26.990
	4	11.44%	1.208	0.0022	1.84%	26.636
	12	8.40%	1.321	0.0025	1.92%	27.045
0.1	1	31.87%	1.195	0.0183	1.5%	26.815
	2	19.51%	1.311	0.0121	0.9%	27.006
	4	18.81%	1.139	0.0598	5.2%	26.386
	12	13.93%	1.309	0.0679	5.33%	27.704

Table 3.4: Simulation result for 4 coplanar symmetric UAVs. Notice that the overall norm of the matrix and the value of λ_{14} remain pretty much untouched by the noise. The value that is most influenced is that of λ_{13} which in itself determines the rigidity of the matrix: it is the threshold value for the rank condition for IBR on the configuration. In this table the ratio between the two eigenvalue is considered as an indication of rigidity, since the rank calculated by Matlab seem not to be robust. The fact that for minimal variance the eigenvalues ratio remains small reinforces the reliability of this performance index. Also note how the norm of the overall matrix is basically untouched by the noise, revealing that is not a so good descriptor of the overall rigidity of the BRM.

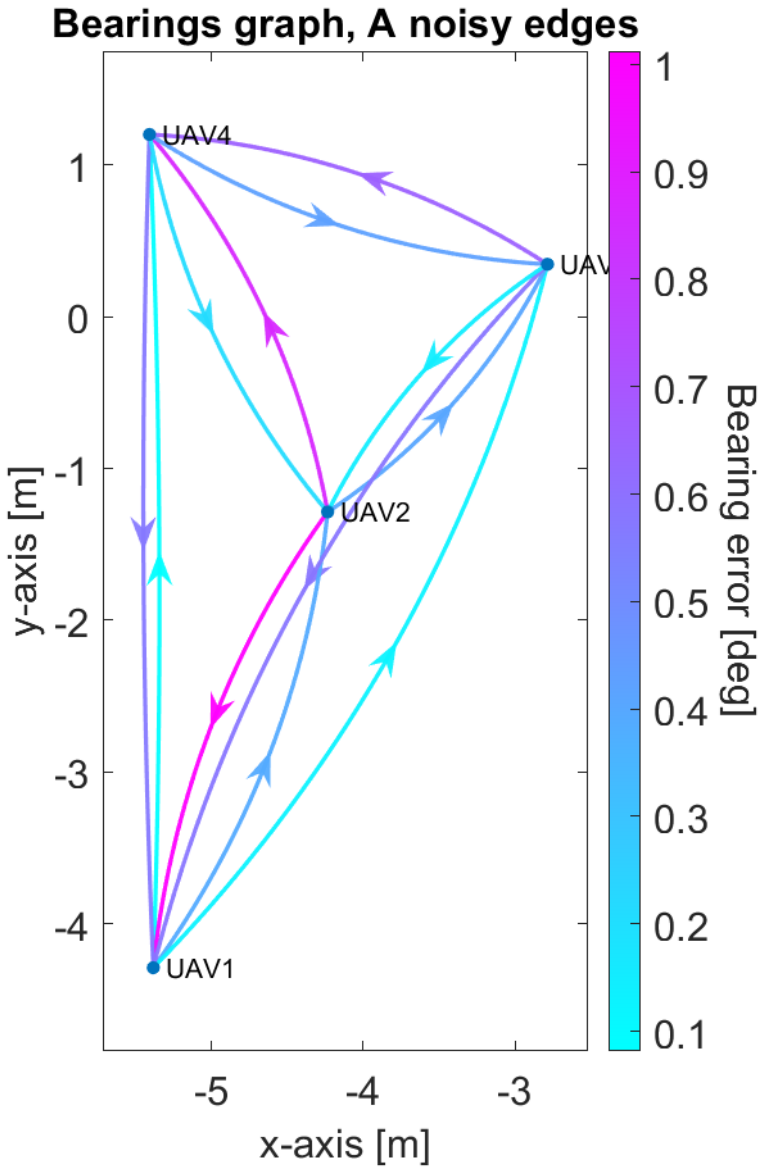

Figure 3.6: Morphed bearing measurement graph of the swarm. Error with variance of 0.06 on all edges. The noise is more or less equally distributed among all edges.

Variance	# Noisy edges	Average error ratio	λ_{14}	λ_{13}	$\lambda_{13}/\lambda_{14}$	$\|\|B\|\|_F^2$
-	0	0	0.0343	$1.6{\cdot}10^{-16} \approx 0$	0%	6.847
0.001	1	0.006%	0.0343	$3.65{\cdot}10^{-10}$	$1.06{\cdot}10^{-6}$ %	6.847
	2	0.032%	0.0343	$5.78{\cdot}10^{-9}$	$1.68{\cdot}10^{-5}$%	6.847
	4	0.039%	0.0343	$1.21{\cdot}10^{-8}$	$3.54{\cdot}10^{-5}$ %	6.847
	12	0.033%	0.0343	$1.97{\cdot}10^{-7}$	$5.76{\cdot}10^{-5}$ %	6.846
0.03	1	0.18%	0.0342	$3.26{\cdot}10^{-6}$	$9.53{\cdot}10^{-4}$ %	6.846
	2	0.98%	0.0341	$5.19{\cdot}10^{-5}$	0.01 %	6.846
	4	1.18%	0.0339	$1.09{\cdot}10^{-5}$	0.03 %	6.846
	12	1.01%	0.0344	$1.79{\cdot}10^{-5}$	0.05 %	6.835
0.06	1	0.37%	0.0341	$1.29{\cdot}10^{-5}$	0.03 %	6.846
	2	1.95%	0.0339	$2.07{\cdot}10^{-6}$	0.06 %	6.846
	4	2.35%	0.0336	$4.342{\cdot}10^{-5}$	0.1 %	6.846
	12	2.02%	0.0346	$7.23{\cdot}10^{-5}$	0.2 %	6.824
0.1	1	0.61%	0.0340	$3.564{\cdot}10^{-6}$	0.01 %	6.846
	2	3.25%	0.0338	$5.733{\cdot}10^{-5}$	0.14 %	6.845
	4	3.91%	0.0333	0.0001	0.32 %	6.845
	12	3.37%	0.0350	0.0002	0.57 %	6.810

Table 3.5: In the case of non-symmetric disposition for the swarm, the matrix starts for an already precarious rigidity without noise. One can easily see that for the same variance as before, the impact on the average error is lower, and this translated into a better ratio between the two eigenvalues when compared with error ratios as the one of the previous table. This means that when the matrix does not offer much rigidity, the impact of the noise is lower.

Variance	# Noisy edges	Average error ratio	λ_{14}	λ_{13}	$\lambda_{13}/\lambda_{14}$	$\|\|B\|\|_F^2$
-	0	0	0.9221	$1.84{\cdot}10^{-15} \approx 0$	0%	16.210
0.001	1	0.084%	0.9227	$8.695{\cdot}10^{-8}$	$9.42{\cdot}10^{-6}$	16.211
	2	0.069%	0.9221	$2.45{\cdot}10^{-7}$	$2.66{\cdot}10^{-5}$	16.207
	4	0.069%	0.922	$4.29{\cdot}10^{-7}$	$4.65{\cdot}10^{-5}$	16.208
	12	0.099%	0.9210	$1.45{\cdot}10^{-6}$	0.0001%	16.219
0.03	1	2.60%	0.9271	$8.12{\cdot}10^{-5}$	0.0087%	16.261
	2	2.05%	0.9203	0.0002	0.02%	16.140
	4	2.06%	0.9301	0.0003	0.04%	16.166
	12	3.01%	0.90715	0.0014	0.15%	16.534
0.06	1	5.31%	0.9336	0.0003	0.03%	16.315
	2	4.02%	0.9194	0.0007	0.08%	16.076
	4	4.10%	0.9376	0.0014	0.15%	16.144
	12	6.05%	0.8904	0.0061	0.68%	16.928
0.1	1	9.11%	0.9416	0.0009	0.10%	16.390
	2	6.52%	0.9177	0.0019	0.21%	15.998
	4	6.79%	0.9468	0.0038	0.41%	16.149
	12	10.19%	0.8651	0.0191	2.21%	17.606

Table 3.6: The scaled disposition exhibits a middle ground between the symmetric disposition and the morphed one.

Homogenous 4 agents fleet UAV, non-coplanar disposition

Same procedure as above is repeated considering a fleet of 4 UGV but his time without forcing a coplanar disposition (fig. 3.7). The maximum bearing angle used in order to compute the average error ratio is the same as before (45 [deg]).

Variance	# Noisy edges	Average error ratio	λ_{14}	λ_{13}	$\lambda_{13}/\lambda_{14}$	$\|\|B\|\|_F^2$
-	0	0	1.3192	1.5387e-15	0	23.971
0.001	1	0.121%	1.3332	3.5686e-07	2.7048e-05%	23.972
	2	0.123%	1.3294	1.311e-06	9.9367e-05%	23.971
	4	0.127%	1.3326	2.3631e-06	0.0001%	23.965
	12	0.132%	1.3281	4.1856e-06	0.0003%	24.008
0.03	1	3.67%	1.323	0.0003	0.024%	23.98
	2	3.66%	1.323	0.0011	0.086%	23.93
	4	3.76%	1.322	0.0020	0.15%	23.80
	12	4.02%	1.324	0.0041	0.31%	25.16
0.06	1	7.42%	1.3332	0.0013	0.10%	23.997
	2	7.24%	1.3294	0.0044	0.33%	23.902
	4	7.48%	1.3326	0.0076	0.57%	23.668
	12	8.21%	1.3281	0.0186	1.40%	26.585
0.1	1	12.507%	1.343	0.004	0.284%	24.011
	2	11.905%	1.336	0.012	0.876%	23.844
	4	12.391%	1.339	0.020	1.501%	23.539
	12	14.111%	1.281	0.064	5.004%	28.966

Table 3.7: Once again, when the bearing error becomes very impactful (10%+ of measurement) the ratio between the eigenvalue reaches an amount over the 1% which at this point can be assimilated to the loss of IBR. It is also of notice that the norm enlarges when all the edges are contaminated by noise.

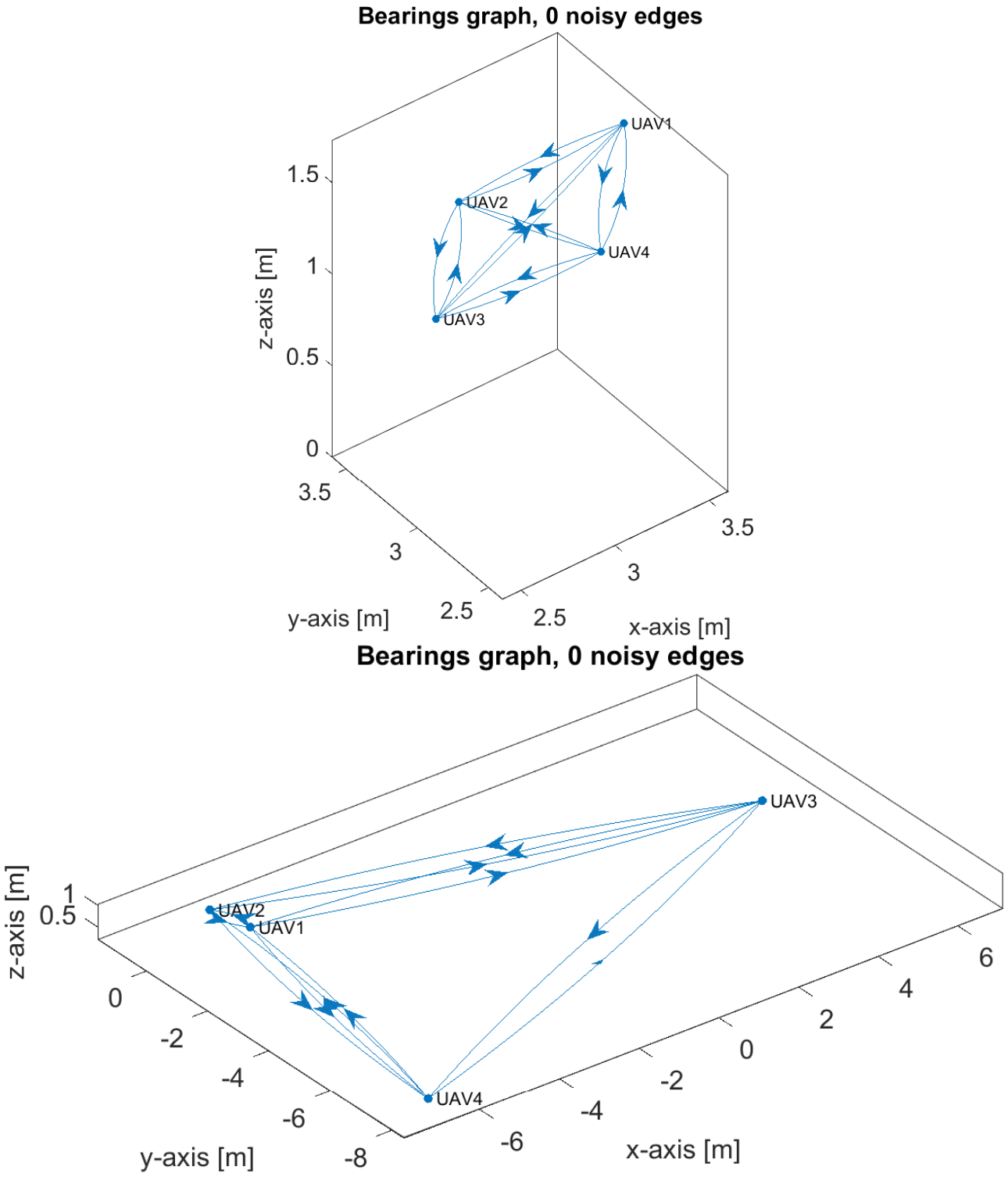

Figure 3.7: Disposition for the second noise experiment. Upper: symmetric configuration. Lower: morphed configuration.

Variance	# Noisy edges	Average error ratio	λ_{14}	λ_{13}	$\lambda_{13}/\lambda_{14}$	$\|\|B\|\|_F^2$
-	0	0	0.010	8.4298e-16	0%	6.489
0.001	1	0.003%	0.011	7.6828e-11	7.2378e-07 %	6.490
	2	0.049%	0.011	1.3648e-09	1.2857e-05 %	6.489
	4	0.024%	0.011	1.6167e-09	1.5231e-05 %	6.489
	12	0.030%	0.011	4.2106e-09	3.968e-05 %	6.490
0.03	1	0.097%	0.011	6.9629e-08	0.001%	6.490
	2	1.453%	0.011	1.1432e-06	0.011%	6.479
	4	0.722%	0.011	1.3721e-06	0.013%	6.473
	12	0.915%	0.011	3.5685e-06	0.034%	6.495
0.06	1	0.194%	0.011	2.8054e-07	0.003%	6.490
	2	2.876%	0.011	4.2119e-06	0.040%	6.467
	4	1.422%	0.011	5.1558e-06	0.049%	6.457
	12	1.843%	0.010	1.3044e-05	0.125%	6.498
0.1	1	0.325%	0.011	7.8685e-07	0.007%	6.490
	2	4.728%	0.011	1.0404e-05	0.098%	6.452
	4	2.323%	0.011	1.3166e-05	0.124%	6.438
	12	3.098%	0.010	3.1227e-05	0.303%	6.498

Table 3.8: Given the morphed disposition presents collinearity, it is possible to observe that λ_{14} has a particularly low value. Once again, the impact of the noise is lessened with respect to the previous simulation, which translates into an higher ratio between eigenvalues in the worst scenario (0.1 variance, all edges), which however does not cross the 1% threshold In this case, the norm enlargement observed previously does not present itself.

Heterogeneous 4 agents fleet

The simulation is now run on a fleet composed of 3 UGVs and 1 UAV. Symmetric and morphed disposition are shown in fig. 3.8. Once again the average bearing error is computed on 45 [deg].

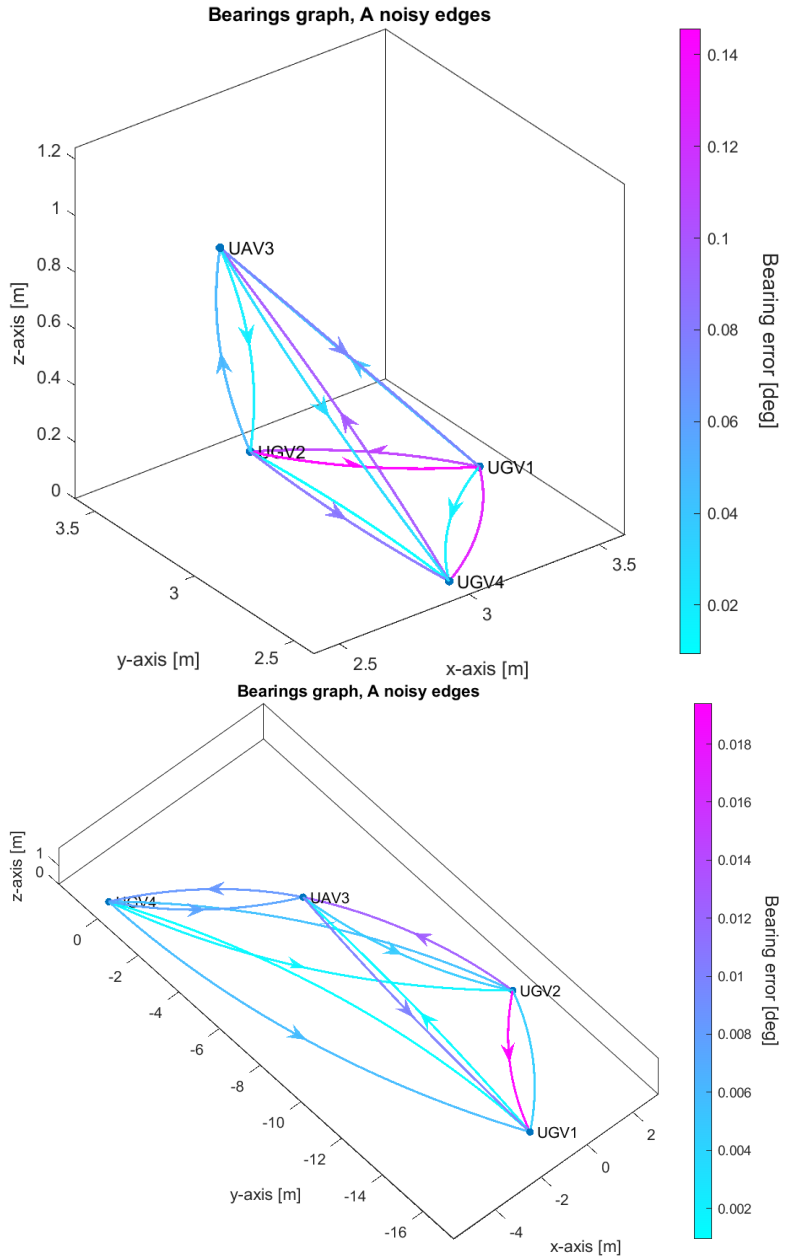

Figure 3.8: Disposition for the third noise experiment. Plot for variance 0.0001 on all edges.

Variance	# Noisy edges	Average error ratio	λ_{14}	λ_{13}	$\lambda_{13}/\lambda_{14}$	$\|\|B\|\|_F^2$
-	0	0%	0.14264	1.6673e-15	0%	17.486
0.001	1	0.12746%	0.14264	2.0212e-07	0.0001417%	17.491
	2	0.094108%	0.14261	6.7007e-07	0.00046986%	17.479
	4	0.088622%	0.14277	6.0121e-07	0.00042111%	17.485
	12	0.14897%	0.14218	4.5893e-06	0.0032279%	17.487
0.03	1	3.9432%	0.14265	0.00019266	0.13506%	17.633
	2	2.7225%	0.14172	0.00051295	0.36196%	17.274
	4	2.6634%	0.14646	0.00053938	0.36829%	17.503
	12	4.4891%	0.12872	0.0047174	3.6648%	17.528
0.06	1	8.1438%	0.14265	0.0008169	0.57266%	17.79
	2	5.2511%	0.14085	0.0017418	1.2366%	17.089
	4	5.3534%	0.15058	0.0022252	1.4777%	17.61
	12	9.0136%	0.11541	0.020674	17.913%	17.569
0.1	1	14.173%	0.14266	0.0024459	1.7145%	18.015
	2	8.356%	0.13979	0.0039218	2.8056%	16.877
	4	9.0242%	0.15665	0.0067213	4.2907%	17.883
	12	15.081%	0.10054	0.056878	56.575%	17.602

Table 3.9: The behavior of the heterogeneous fleet is completely different from the ones observed up to this point. The low variance simulation behaves as usual, but as soon as the variance rises a bit, even for average error ratios comparable to the previous ones, the effect of an all-noisy graph is very apparent, shifting λ_{14} by a great amount in addition to λ_{13} and thus affecting the ratio between the two. This phenomenon presents itself only when all the edges are affected by noise, as can be observed in the discontinuity $4 \rightarrow 12$ in the eigenvalue ratio, which is out of scale when considering the previous simulations.

Variance	# Noisy edges	Average error ratio	λ_{14}	λ_{13}	$\lambda_{13}/\lambda_{14}$	$\|\|B\|\|_F^2$
-	0	0%	0.0017821	1.1211e-17	0%	5.9192
0.001	1	0.0030418%	0.001782	5.738e-12	3.2199e-07%	5.9192
	2	0.017738%	0.0017821	1.6076e-10	9.0211e-06%	5.9192
	4	0.016314%	0.0017822	1.3417e-10	7.5284e-06%	5.9193
	12	0.015235%	0.0017826	7.4705e-10	4.1908e-05%	5.9192
0.03	1	0.091103%	0.0017811	5.1503e-09	0.00028917%	5.9192
	2	0.53241%	0.0017822	1.4632e-07	0.0082102%	5.9191
	4	0.48862%	0.0017845	1.2166e-07	0.0068173%	5.9199
	12	0.45706%	0.0017979	6.7197e-07	0.037375%	5.9196
0.06	1	0.1819%	0.0017801	2.0544e-08	0.0011541%	5.9192
	2	1.0653%	0.0017824	5.9196e-07	0.033211%	5.9189
	4	0.97557%	0.0017871	4.9033e-07	0.027437%	5.9205
	12	0.91415%	0.0018153	2.6844e-06	0.14788%	5.9198
0.1	1	0.30247%	0.0017787	5.6857e-08	0.0031965%	5.9192
	2	1.7766%	0.001783	1.6686e-06	0.093583%	5.9187
	4	1.6222%	0.0017908	1.3755e-06	0.076812%	5.9214
	12	1.5237%	0.0018409	7.4349e-06	0.40388%	5.92

Table 3.10: Considering what happened for the symmetric configuration, it is worth noticing that the non-symmetric one consistently exhibits more resilience to the effect of the noisy measurements. The discontinuity which can be observed in the eigenvalues ratio $4 \to 12$ is still present, however with a lesser degree than before, given in the worst case scenario the ratio goes $0.07 \to 0.40$ ($5\times$) while before it went $4.2 \to 56.5$ ($14\times$).

Homogenous 14 agents fleet UAV, planar disposition

Finally, to illustrate how the cardinality of the agents relates to noise, a symmetric planar swam of 14 UAVs is tested as seen in fig. 3.9. Since the graph has $n \cdot (n-1) = 182$ edges, the noisy will characterize a different amount of measurements: 1, 10, 30 and 100 edges. The maximum bearing considered will be $180/14 = 12.8[deg]$ and also the variances will be different, accounting for the new maximum bearing.

Variance	# Noisy edges	Average error ratio	λ_{34}	λ_{33}	$\lambda_{33}/\lambda_{34}$	$\|\|B\|\|_F^2$
-	0	0%	5.1709	4.9897e-14	9.6495e-13%	711.95
0.001	1	1.3797%	5.1705	3.9399e-05	0.000762%	711.48
	10	1.2092%	5.1702	7.5433e-05	0.001459%	711.63
	30	0.93256%	5.1721	0.00014703	0.0028427%	712.58
	100	1.1136%	5.1638	0.00042042	0.0081417%	711.58
0.009	1	12.242%	5.166	0.0029404	0.056919%	707.86
	10	10.839%	5.0456	0.0059914	0.11874%	708.96
	30	8.448%	5.1257	0.012249	0.23897%	718.64
	100	10.027%	4.9664	0.034345	0.69154%	709.38
0.018	1	24.059%	5.1599	0.010446	0.20245%	704.03
	10	21.57%	4.9115	0.023339	0.47519%	705.81
	30	17.032%	5.0234	0.05071	1.0095%	727.69
	100	20.061%	4.7707	0.1374	2.8801%	708.09
0.03	1	39.086%	5.1504	0.024276	0.47134%	699.27
	10	35.685%	4.8745	0.061879	1.2695%	701.36
	30	28.723%	4.9394	0.14778	2.9919%	743.83
	100	33.437%	4.6111	0.37338	8.0973%	707.89

Table 3.11: Of course, being that the swarm now has more components, the inter-agent bearing angles will be smaller and denser. This means that maintaining the previous variance would cause an unrealistic and unsustainable amount of error, which can still be observed here on the last case with variance 0.018 - 0.03. Apart from this issue, the behavior seems to retrace the one of the 4 agent configuration.

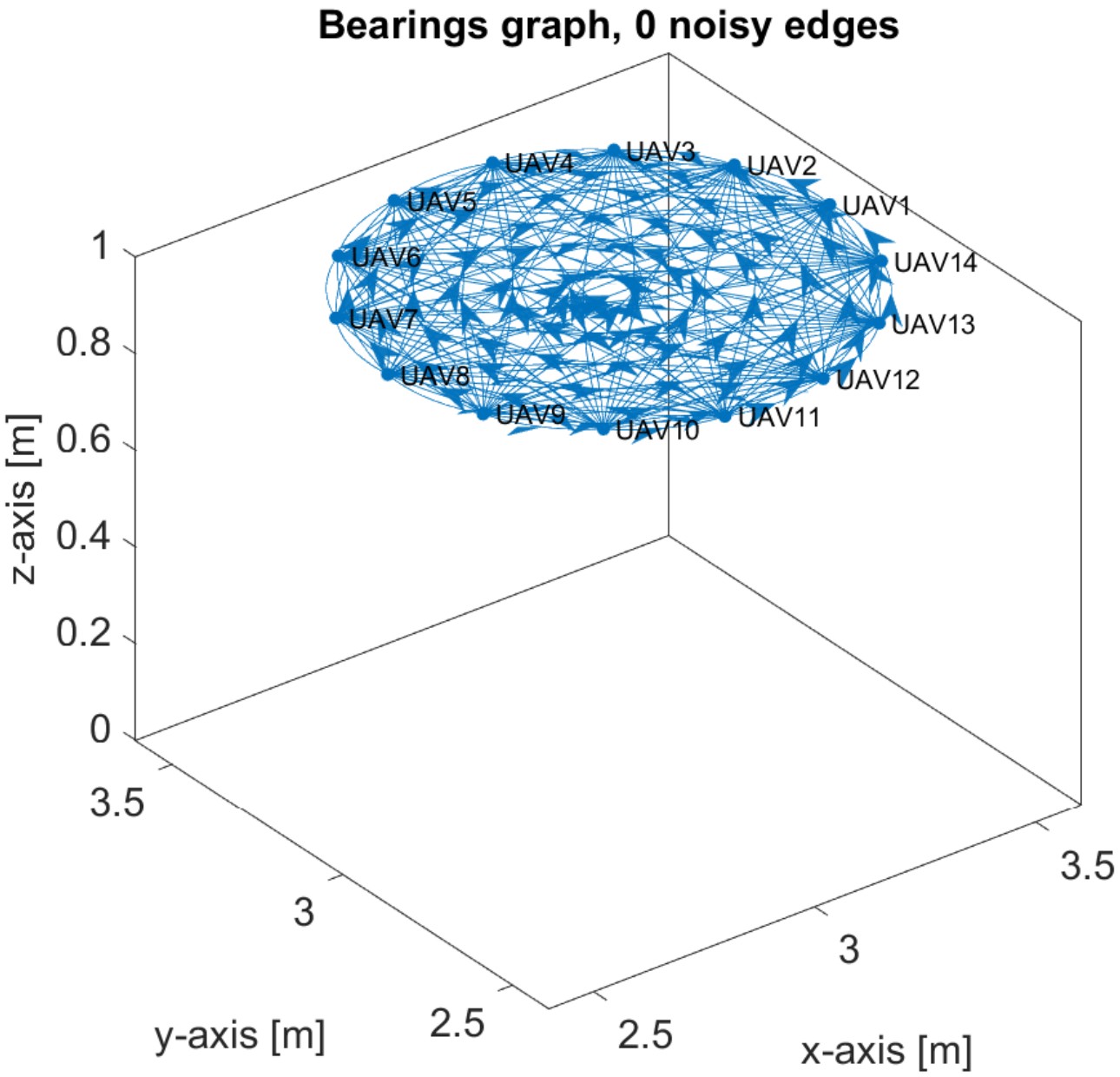

Figure 3.9: Formation of 14 UAVs considered.

Chapter 4

Conclusions

This effort allowed ascertaining that the procedure to build the unified bearing rigidity matrix works as intended. Such procedure can be readily implemented in a programmatic fashion and generalized for any manner of agent in $SE(3)$ and for any cardinality. In addition, the theoretical rank requirements of the matrix have been confirmed in all considered noiseless configuration. In particular, the fact that trivial variations are spanned by the kernel of the BRM has been confirmed. That said, it is also apparent that rigidity is not a binary feature, but instead has direct dependence on the value of the smallest non-null eigenvalues of the SBRM. Symmetric disposition of agents has been shown to exhibit greater rigidity than the non-symmetric counterpart, in particular it has been confirmed that distances, and not only pure orientations, play an important part in the rigidity characteristics. Near-collinear configuration correspond to critical amount of rigidity, if any. The norm of the BRM seem to have direct correlation with the amount of edges w.r.t. a complete graph condition. As for the experimentation concerning bearing measurement error, it has been confirmed that it has a far greater effect on a symmetric configuration starting for a stronger rigidity condition than on a less rigid formation. The norm of the BRM remains relatively untouched by the error effect, as does the second to last non-null eigenvalue, which is effected only in the case the error amount is comparable with measurement itself. Noise seem to have a greater effect on inherently more rigid configurations (in particular symmetric one), while starting from a lesser degree of rigidity give more resilience to bearing error. Heterogeneous configurations appear to be particularly exposed to the effect of noise whenever the entirety of the graph is affected, or at least more so than homogenous ones. Finally, the more agents there are in a formation, the more the relative bearing angles will be small. Therefore, if the same bearing error amount would be applied to two different fleets, the one with a lesser number of agents will be affected the least regarding its rigidity characteristic: the more numerous the fleet, the more prone to errors.

Bibliography

[1] Hyo-Sung Ahn *Formation Control: approaches to distributed agents.*, Springer 2020.

[2] M. De Queiroz, X. Cai, M. Feemster *Formation control of multi-agent systems: a graph rigidity appraoch*, Wiley 2019

[3] G. Michieletto, A. Cenedese, D. Zelazo *A unified dissertation on bearing rigidity theory*, IEEE Trans. Robot. 2021

[4] A. Cenedese, G. Michieletto *Heterogenous formation control in presence of noisy measurements*, ECC 2022 WS

[5] G. Michieletto, A. Cenedese, A. Franchi *Bearing rigidity theory in SE(3)*, IEEE CDC 2016

[6] D. Zelazo, A. Cendese *Foundaions of formation control*, 2019

[7] S. Zhao, D. Zelazo *Bearing rigidity theory and its applications for control and estimation of network systems: life beyond distance rigidity*, IEEE CSM 2019

[8] G. Zhu, J. Hu *Stiffness matrix and quantitative measure of formation rigidity*, IEEE CDC 2009

[9] B. Pozzan, G. Michieletto, A. Cenedese, D. Zelazo *Heterogenous formation control: a bearing rigidity approach*, IEEE CDC 2021

[10] F. Schiano, A. Franchi, D. Zelazo, P. R. Giordano *A Rigidity-Based Decentralized Bearing Formation Controller for Groups of Quadrotor UAVs*, IEEE IROS 2016